INTEGRATED RESERVOIR STUDY OF THE 8 RESERVOIR

OF THE GREEN CANYON 18 FIELD

A Thesis

by

ANTHONY UDEGBUNAM ANIEKWENA

Submitted to the Office of Graduate Studies of
Texas A&M university
in partial fulfillment of the requirements for the degree of

MASTER OF SCIENCE

August 2003

Major Subject: Petroleum Engineering

INTEGRATED RESERVOIR STUDY OF THE 8 RESERVOIR

OF THE GREEN CANYON 18 FIELD

A Thesis

by

ANTHONY UDEGBUNAM ANIEKWENA

Submitted to Texas A&M University
in partial fulfillment of the requirements
for the degree of

MASTER OF SCIENCE

Approved as to style and content by:

Duane A. McVay (Chair of Committee)	W. John Lee (Member)
Wayne M. Ahr (Member)	Hans C. Juvkam-Wold (Head of Department)

August 2003

Major Subject: Petroleum Engineering

ABSTRACT

Integrated Reservoir Study of the 8 Reservoir of the Green Canyon 18 Field.

(August 2003)

Anthony Udegbunam Aniekwena, B.E., University of Nigeria, Nsukka

Chair of Advisory Committee: Dr. Duane A. McVay

The move into deeper waters in the Gulf of Mexico has produced new opportunities for petroleum production, but it also has produced new challenges as different reservoir problems are encountered. This integrated reservoir characterization effort has provided useful information about the behavior and characteristics of a typical unconsolidated, overpressured, fine-grained, turbidite reservoir, which constitutes the majority of the reservoirs present in the Outer Continental Shelf of the Gulf of Mexico.

Reservoirs in the Green Canyon 18 (GC 18) field constitute part of a turbidite package with reservoir quality typically increasing with depth. Characterization of the relatively shallow 8 reservoir had hitherto been hindered by the difficulty in resolving its complex architecture and stratigraphy. Furthermore, the combination of its unconsolidated rock matrix and abnormal pore pressure has resulted in severe production-induced compaction.

The reservoir's complex geology had previously obfuscated the delineation of its hydrocarbon accumulation and determination of its different resource volumes. Geological and architectural alterations caused by post-accumulation salt tectonic activities had previously undermined the determination of the reservoir's active drive mechanisms and their chronology.

Seismic interpretation has provided the reservoir geometry and topography. The reservoir stratigraphy has been defined using log, core and seismic data. With well data as pilot points, the spatial distribution of the reservoir properties has been defined using geostatistics. The resulting geological model was used to construct a dynamic flow model that matched historical production and pressure data..

The reservoir's pressure and production behavior indicates a dominant compaction drive mechanism. The results of this work show that the reservoir performance is influenced not only by the available drive energy, but also by the spatial distribution of the different facies relative to well locations. The study has delineated the hydrocarbon bearing reservoir, quantified the different resource categories as STOIIP/GIIP = 19.8/26.2 mmstb/Bscf, ultimate recovery = 9.92/16.01 mmstb/Bscf, and reserves (as of 9/2001) = 1.74/5.99 mmstb/Bscf of oil and gas, respectively. There does not appear to be significant benefit to infill drilling or enhanced recovery operations.

DEDICATION

I dedicate this work first to God, the Almighty, for all His loving kindness to me in spite of myself. He has been my life, my sustenance, my all. Of the same God, who has given me so much, I ask two things: a grateful heart, and a humble and obedient spirit.

I dedicate it to my late parents, Clement and Catherine Aniekwena, for their incomparable love and the guidance they gave me.

I dedicate it to my senior brother, Michael Obiora Aniekwena, and his wife, Evelyn. Since my early childhood, Michael, like my parents, has been untiring in urging and encouraging me to acquire knowledge and wisdom.

I also dedicate it to my children for their faith and belief in me: my eight year old son, Adriaan Nebeolisa Aniekwena, and my six year old daughter, Stephanie Ifeyinwa Aniekwena, for their unconditional love and understanding.

ACKNOWLEDGEMENTS

I express my sincere gratitude to Dr. Duane A. McVay, chairman of my advisory committee for his guidance and support throughout this research. I am grateful for the strength and sense he gave me. I thank my committee members, Dr. W. John Lee and Dr. Wayne M. Ahr for being there for me all the time.

I am indebted to Dr. Thomas Blasingame, the Graduate Advisor in the Petroleum Engineering Department, for the "human face" he showed in his office by caring not only for the progress of the department, but also for the well-being of the students. I thank the faculty and staff of the Petroleum Engineering Department; my association with them has been very rewarding in many ways.

I am grateful to my pragmatic brother, Patrick, and his wife, Patricia, and also my other siblings and their families for supporting me during the last two years, even if they were far away from me.

I thank the geoscientists, S. Lalande and M. Plantevin, who started off this research and "paved the way in the desert" towards the realization of this study. I gratefully acknowledge all my friends at Texas A&M with whom I shared my happy and sad moments.

TABLE OF CONTENTS

LIST OF TABLES

LIST OF FIGURES

FIGURE Page

FIGURE Page

CHAPTER I

INTRODUCTION

Project Overview

The Gulf of Mexico is a major petroleum-producing province with considerable importance to the U.S. economy. A significant proportion of the reservoirs in the Outer Continental Shelf of the Gulf of Mexico consist of thin-bedded deposits of submarine fan systems. These reservoirs are typically very heterogeneous, consisting of turbidite channel deposits combined with sheet-like levee and overbank deposits. They are often heavily faulted. Their stratigraphic features are subtle and difficult to detect because sand response is often close to shale response except where they are cut by channels.

Weimer *et al.*[1] suggested that because turbidite reservoirs are usually more complex than expected, their production performance is considerably different from predicted performance. They stressed the need for integrated management of this type of reservoirs.

The Green Canyon 18 field is an intermediate submarine fan system with reservoir quality typically prograding with depth[2] (Fig. 1). The main pay consists of the numbered sands 8 to 30, occurring within the depth range 9,500 ftss and 13,900 ftss.

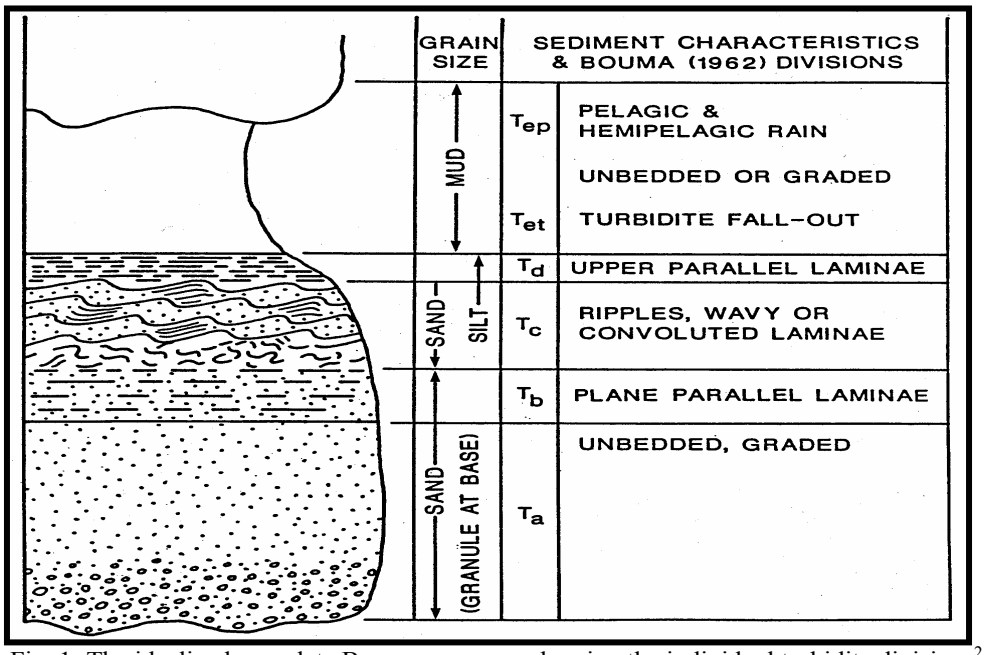

Fig. 1: The idealized complete Bouma sequence showing the individual turbidite divisions[2].

This thesis follows the style of *SPE Reservoir Evaluation & Engineering* journal.

Reservoir Development History

Green Canyon Block 18 (GC-18) is a 5888-acre block located some 70 miles off the Louisiana coast, approximately 120 miles south of Morgan City (Fig. 2).[3] The Green Canyon Block 18 field was discovered in 1982. The field, which is operated by ExxonMobil, is a four-partner joint venture. All wells in the field were drilled from a single platform located to the south of the field[4] (Fig. 3). All the wells are therefore high angle and deviated, most with 'S' profiles and a few being extended-reach wells. The 900-ft production platform was set in November 1986 in 760 feet of water. Since May 1987, it has been under simultaneous drilling and production operations. The platform capacity is 22,000 and 25,000 bpd of oil and water, respectively, and 45,000 to 60,000 Mscfpd of gas. Its gas compression capacity is 19,000 Mcfpd. As of end 1996, some 30 wells have been drilled, with two of them considered expendable.

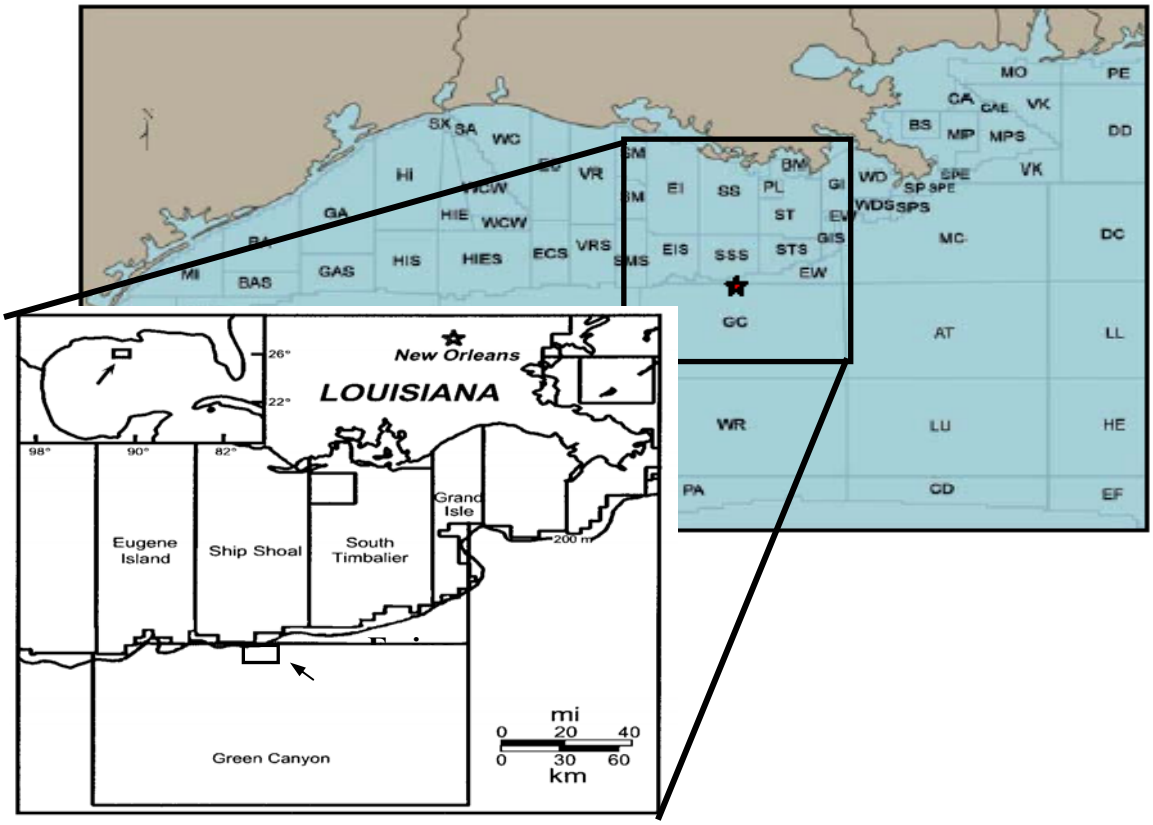

Fig. 2: Location of the Green Canyon 18 field (after Weimer *et al.*, 1998)[3], magnified from the Northern Gulf of Mexico map showing the Outer Continental Shelf leasing area.

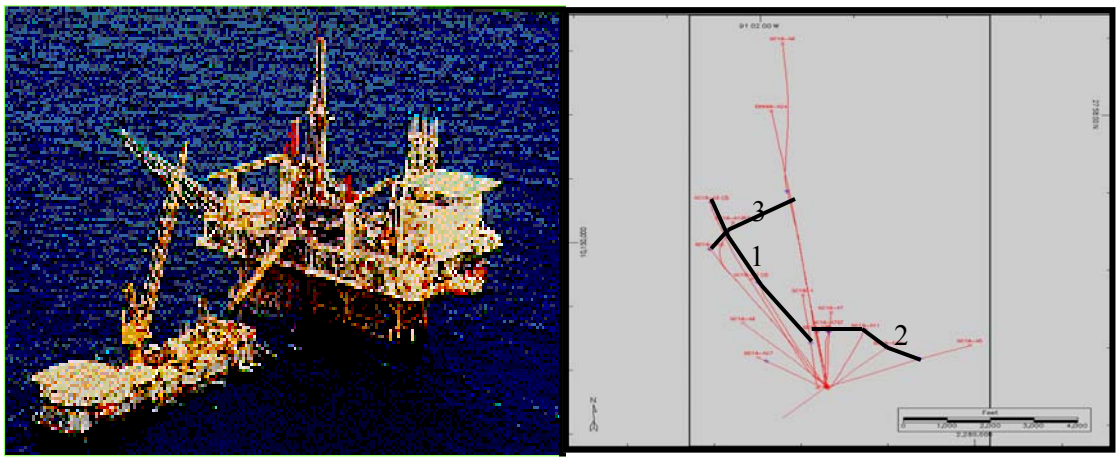

Fig. 3: The single drilling and production platform is located to the south of the field[4,5,6].

Background

The economic exploitation of hydrocarbons from the shallower horizons had, hitherto, been hindered by the complex architecture and stratigraphy of the reservoirs and difficulties in resolving them with seismic data.

The 8 reservoir consists of vertical and lateral alternations of sand and shale. The rock matrix is unconsolidated and the pore pressure is above normal. As a result, the reservoir has high pore volume compressibility and has experienced severe compaction since its early production life. The resulting unstable formation has caused different operations problems, especially well failures.

The complex architecture and stratigraphy of the reservoir had, before this study, obfuscated the delineation of its hydrocarbon accumulation, leading to serious uncertainties in the quantification of different resource categories. This complex nature of the reservoir had also made it difficult to predict facies distributions and determine optimum well locations.

Previous Work on the 8 Reservoir

Over sixty different works on all levels of the field have been carried out since 1984.[5] The studies include "Petrology of the sands in Well 2" in April 1984, "Reservoir Simulation Study of the 20 sand" in September 1986, "Development Drilling & Producing Strategy Report" in September 1986, "Special Core Analysis for Well 7" in September 1987, "Sedimentological & Reservoir Analysis of Late Pliocene Core from wells 1 and 9" in July 1988, "Gas Analysis Report" in February 1989, "Formation Compressibility of the 8 & 20 sands" in November 1992, "Integrated Field Study to Determine a Methodology for Evaluation & Development of GC-18 Field" in December 1994, and a material balance study of the 8 reservoir in 2000.

Drilling and seismic results had alluded to the complex architecture and stratigraphy of the 8 reservoir. All work done before this study had been useful general descriptions of the reservoir, or localized quantification of the reserves from decline curve analysis. The material balance study, because it is zero-dimensional, fell short of delineating the hydrocarbon accumulation and defining the spatial fluid distribution in the reservoir for further development activities.

The most recent studies of this reservoir, of which this dynamic simulation is the concluding part, were carried out in Texas A&M University in years 1999-2002. In 2001-2002, an integrated geological and geophysical study[6,7] was carried out, the overall objective of which was to characterize the reservoir to provide a geological model for numerical simulation work.

Reservoir Description

The Gulf of Mexico is peculiar for its intense tectonic activities in the forms of salt movements and growth fault displacements during deposition. These affect the structural development and the depositional pattern of the reservoirs. Studies have been carried out in the past to determine the relationships between salt movement, growth fault development and sediment loading in order to better characterize turbidite reservoirs.[8- 10]

Geological Setting

The environment of deposition in the Outer Continental Shelf of the Gulf of Mexico is greatly influenced by salt tectonic activities.[9,11] Green Canyon 18 represents a channel-levee-overbank system deposited between shallow salt bodies.[6] Deposition of the 8 reservoir resulted from fine-grained turbidity currents in a mid-basin slope.[7] Fig. 4 shows the possible position of GC-18 on a submarine fan system, while Fig. 5 is a conceptual model of a complete system. Reservoir extent and sand quality distribution are controlled by the dominant energy of deposition, which in this environment is identified to be gravity flows.

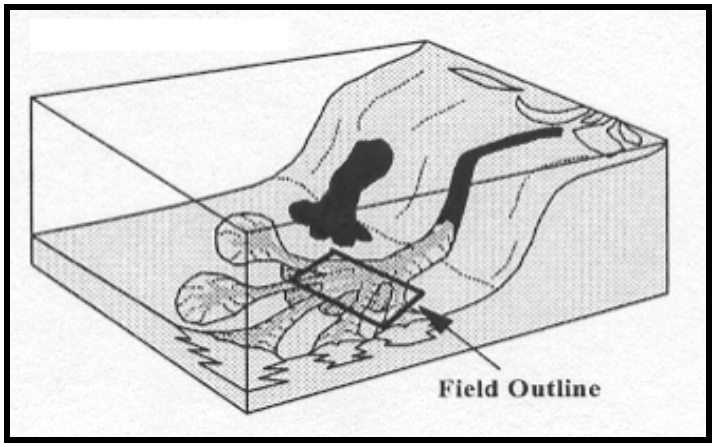

Fig. 4: The depositional environment of the 8 reservoir (modified from Davies *et al*., 1999).[15]

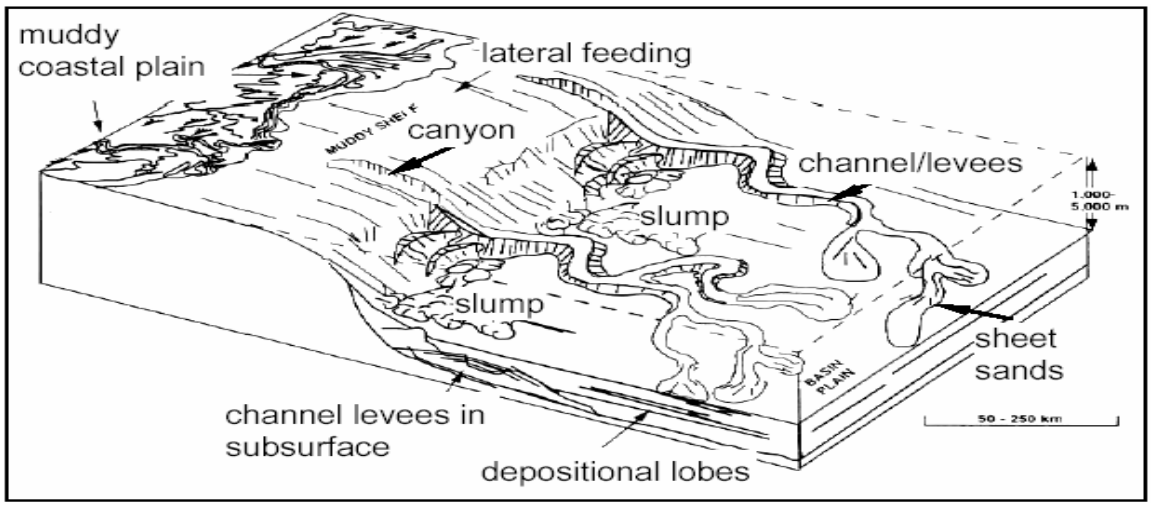

Fig. 5: Conceptual model of a mud-rich turbidite system, with the main architectural elements: modified from Reading and Richard (after Varnai[12]).

Structure

The 8 reservoir structure is a north-northwest-plunging anticline bounded to the south by a northwest-southeast trending, southwest dipping salt-detachment fault. The crest of the structure is located along the fault. The northward plunge of the structure is opposite the regional basin southerly paleo-dip as a result of salt tectonic activities to the south.[6] The top surface of the 8 reservoir lies between 9500 ftss and 10,500 ftss, and when viewed from above, appears approximately trapezoidal in shape (Fig. 6).

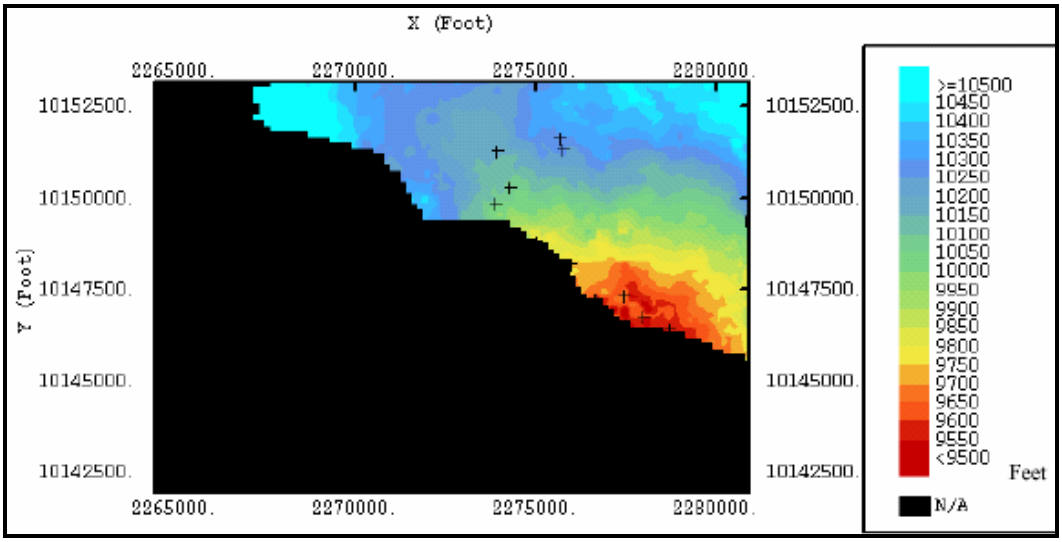

Fig. 6: Structural map of the top of the 8 reservoir (after Lalande[6]).

Stratigraphy

The 8 reservoir consists of assemblages of individual turbidite systems typically representative of a channel-levee depositional environment. Stacking occurs both vertically and laterally and influences the continuity of the sand bodies.[7] This type of stacking is also known as a compensational stacking sequence.

The stratigraphic features of the sand are very subtle and difficult to detect, as individual channels are below seismic resolution. In interpreting the logs for facies discrimination, sand bodies greater than or equal to 2 ft were assumed to be channel fills. In some wells the log response was very close to the shale response.[7]

Two lateral zones with different average properties were delineated using net thickness data derived from log and seismic. Three facies, namely channel, levee and overbank deposits (labeled A, C, and E in Fig. 7) were identified in both zones based on petrophysical interpretations.[9] In modeling the reservoir, property distributions have been constrained to the facies distributions.

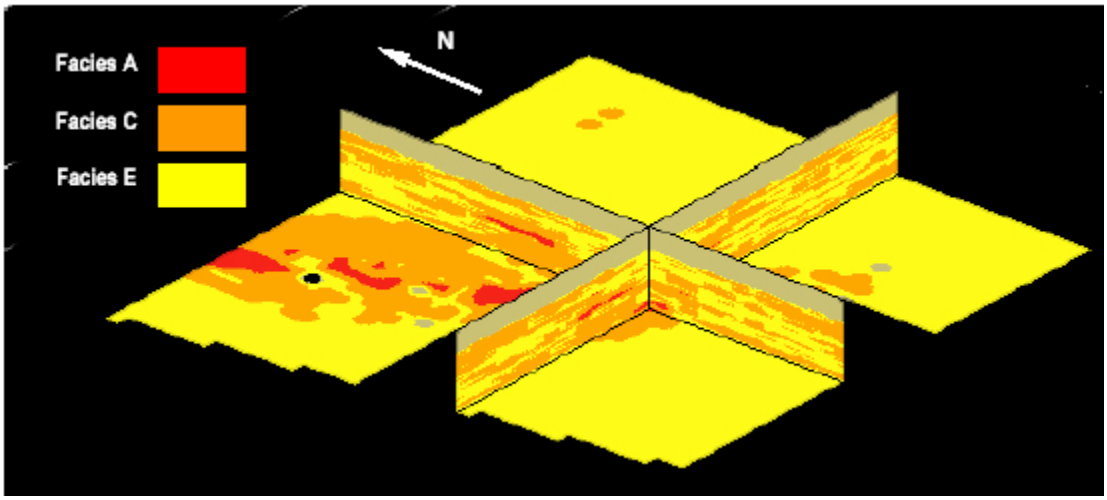

Fig. 7: 3D geostatistical simulation result of the 8 reservoir (after Lalande[6]). The lateral continuity is good, but the vertical continuity varies.

Channels are defined as long-lived sediment pathways that are both erosional and depositional features.[6,13-15] Levee deposits are fine-grained laminated sands and can show the best porosity-permeability combination in the system.[6, 11] Overbank deposits are low sand/shale ratio intervals of the levees, so called "low pay, low resistivity sands."[6,7,14]

Production History

The GC-18 field has enjoyed continuous development since 1982. To date thirty wells have been drilled in the field, of which twenty-six penetrated the 8 reservoir. The field came on stream in May 1987, but the 8 reservoir started producing in November 1987. Production from the 8 reservoir has been from seven wells, namely wells 2, 3, 6, 7, 9, 12, and 25. By 1998 most of the wells were shut in for various reasons, primarily high water-cut and low productivity. As of August 2002, only two wells (wells 2 and 12) were producing, but at high GOR's and high WOR's. As of September 2001, cumulative oil production was 8.18 mmstb (Fig. 8).

Production from the reservoir started from well 3 in December 1987. Production from this well peaked at ca 1800 bopd about a year after first oil, but began to steadily decline almost immediately. Well 12 came on stream some 10 months after well 3. Production from well 12 peaked some 10 months later at ca 1000 bopd. Like well 3, the production from well 12 began a steady decline almost immediately after it reached its peak.

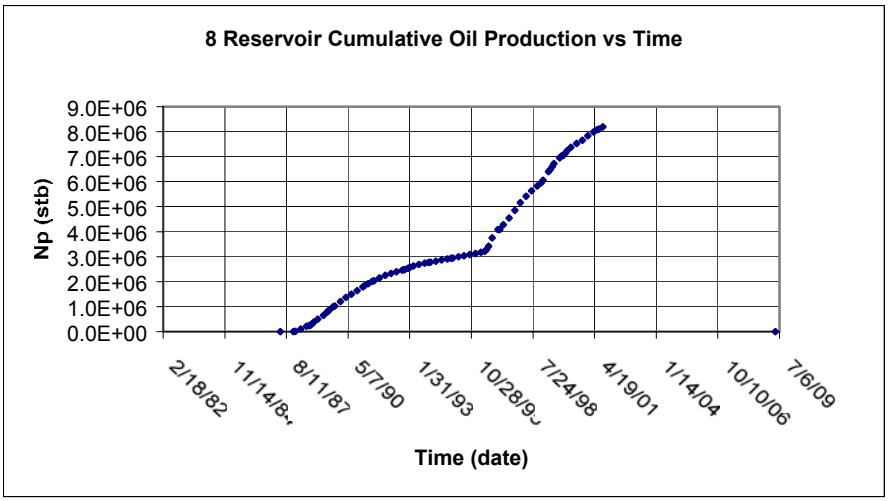

Fig. 8: Plot of cumulative production, N_p, vs Time (date) for the 8 reservoir.

Withdrawal from the reservoir was greatly boosted by mid-1996 when wells 6 and 7 were brought on stream in quick succession. Well 6 proved to be a prolific producer, quickly reaching its peak of over 3600 bopd a few months after coming on stream, and reaching a cumulative oil production of 2.636 mmstb about 3.7 years after coming on stream. Well 7 did not perform as well. Well 2 also contributed significantly to the recovery from the reservoir.

Specific Objectives

The major goal of this study is to gain an understanding of the static and dynamic behaviour of this reservoir by integrating geological, geophysical, fluid PVT, production and pressure data. The aim is to obtain a representative 3D geological model that reproduces the production and pressure performance of the reservoir, and then use the model to determine an optimal development strategy for this reservoir. To achieve this, some specific objectives need to be met:

1. Using a dynamic simulator, calibrate the available 3D geologic model using history matching,
2. Identify and evaluate key uncertainty parameters,
3. Identify dominant and subordinate drive mechanisms and the chronology of their occurrence,
4. Predict the future performance of the reservoir using the calibrated 3D model under different development and production scenarios, and
5. Select a best-case development option, among the alternatives considered, for further development of the reservoir.

CHAPTER II

DATA EVALUATION, ANALYSIS AND INTERPRETATION

In this study, we have tried to honor and use all data available. PVT data have been used as is without any alterations. Petrophysical and geological data were used as is in the initial simulation runs. Their alterations have resulted from model optimization efforts in order to match the observed production data. The key reservoir data validated in this simulation is summarized in the reservoir data sheet in Chapter VI - Results.

The 8 reservoir was initially undersaturated with an initial pressure of 7910 psia at the reservoir datum of 10,000 ftss. The bubble point pressure is 7,750 psia.[4] The oil is light with a gradient of 0.3747 psi/ft (ca 32^{o} API). Data available include 3D seismic data, log derived petrophysical data, special core analysis data (on wells 1 and 7), PVT data, and production data up to 10/1999 (pressures) and 8/2001 (rates).

Petrophysical Data

An evaluation of the petrophysical data and their distribution in the 8 reservoir was done recently and reported in reference 7. Due to the environment of deposition of the reservoir, the 8 reservoir has both a complex architecture and small-scale heterogeneities. Cores of the 8 sand taken in the six wells 7, 8, 11, 12, 25, and 27 portray these small scale heterogeneities.[7] In the computation of the net-to-gross ratio, spontaneous potential (SP) and neutron-density logs were used. Gamma-ray logs were discarded for this purpose because of the high gamma ray response. However, the accuracy of the calculations with the SP and neutron-density logs is subject to tool resolution, which in this case is sub-optimal for the finely laminated sand-shale sequence forming the small-scale vertical heterogeneities. Core-derived porosity showed a wider range (17% - 43%) than log-derived porosity (25% - 38%) for all the facies.

Core and Log Analyses

The 8 sand is generally heterogeneous and consists of thin laminations of sand and shale, which constitute the more ubiquitous levee and overbank deposits. Due to the thin laminations and the coarser logging tool resolution, log response is subtle and it is difficult to discriminate between sand and shale in some wells. Figs. 9, 10 and 11 show three examples of 8 reservoir log responses.[7]

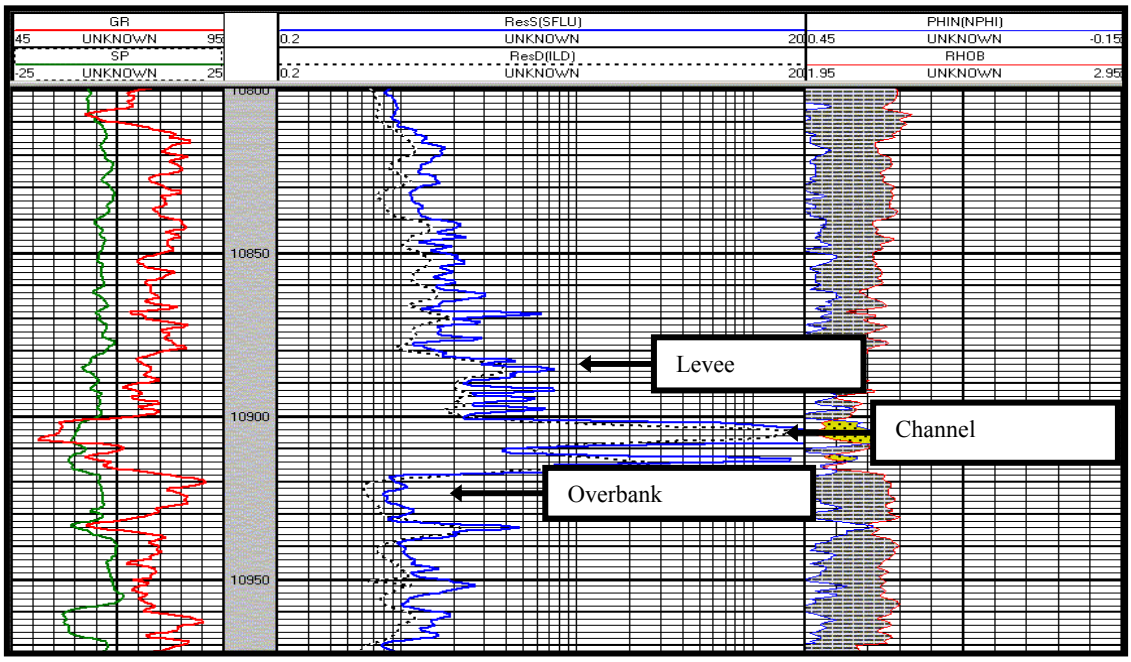

Fig. 9: Log response of the 8 sand interval in well 2. The depths are in ft MD. Note the channel fill interval between 10900 and 10909 ft.

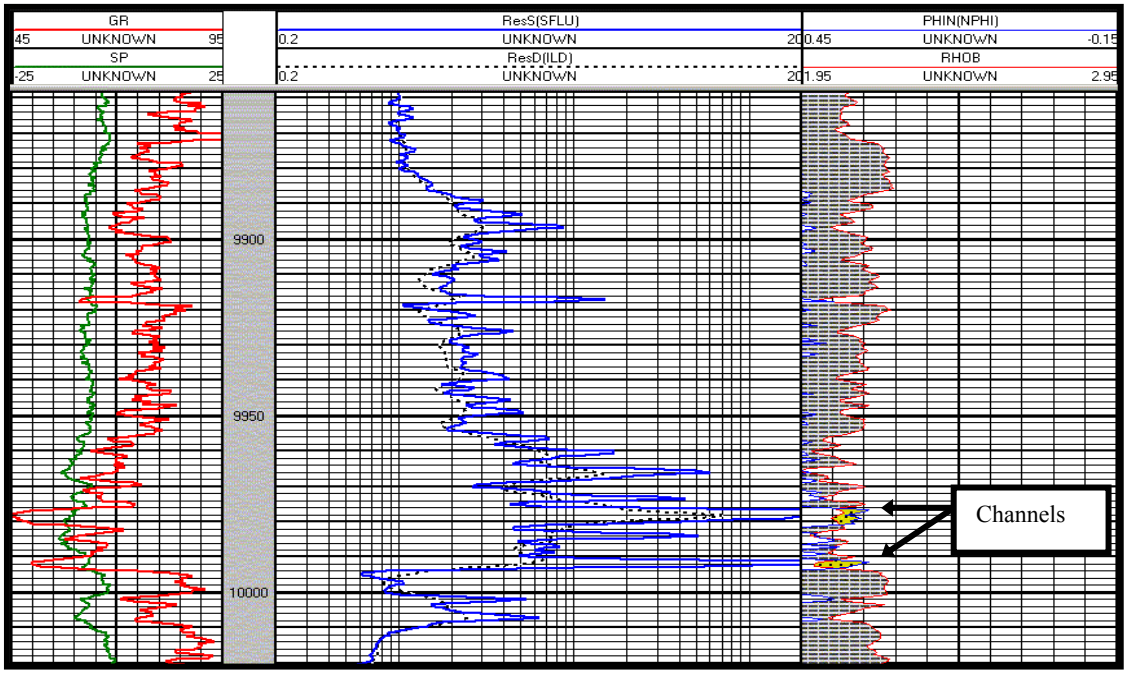

Fig. 10: Log response of the 8 sand interval in well 25. The depths are in ft MD.

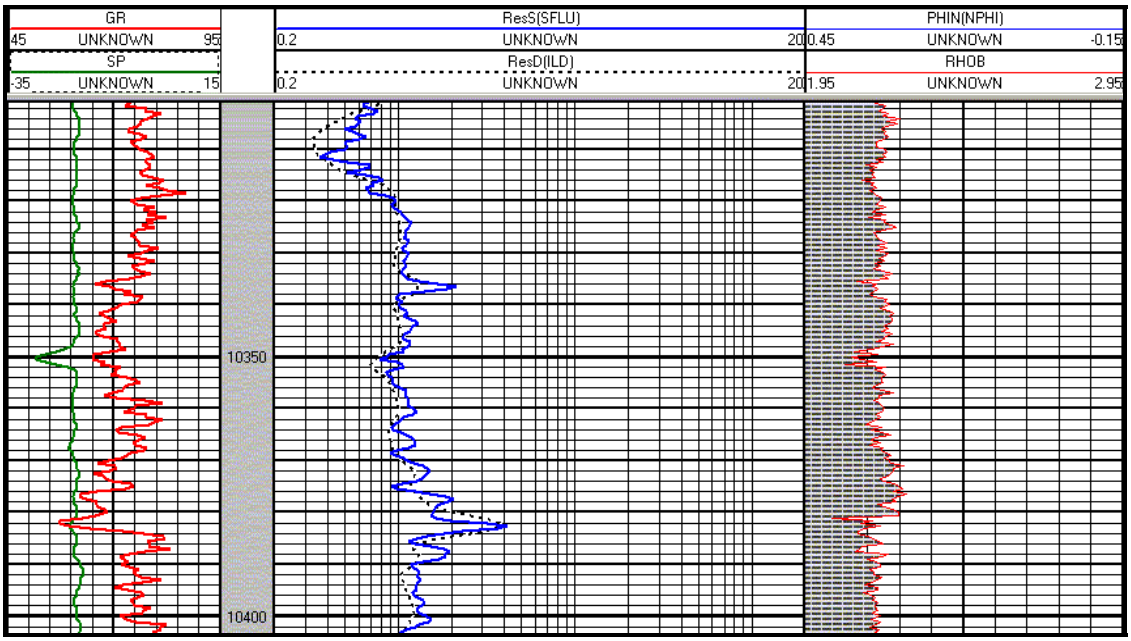

Fig. 11: Log response of the 8 sand interval in well 5. The depths are in ft MD.

Facies Discrimination

The facies were classified based on their log response tied to their appearance on cores. The three classes correspond to channel, levee and overbank deposits. The combination of core and log data provided the criteria for facies discrimination. These criteria are tabulated in Table 1 below. In interpreting the logs for facies discrimination, sand bodies greater than or equal to 2 ft are assumed to be channel fills.[10]

Table 1: Criteria for facies discrimination (after Plantevin).[7]

	Gamma-Ray log	Resistivity log	Density-Neutron log
Channel	Low, less than 60 API	More than 20Ω.m	Inversion of the Neutron and Density curves (decrease of the Neutron porosity value)
Levee	Around 75 API	Between 2 and 10 Ω.m	Close to the shale response, Neutron and Density curves are close.
Overbank	More than 80 API, very close to shale response	Less than 2 Ω.m	Neutron-Density difference higher than for levee deposits

The following characterizes each of the facies:[6,7]

Facies A: Thick intervals (> 5 inches) of clean channel sands sparsely laminated by shales. It has high net-to-gross ratios averaging about 81%.

Facies C: Typical laminated levee sands. The thickness of each sand layer ranges from 0.2 to 5.0 inches. Net-to-gross average is 54%.

Facies E: Shale dominated overbank deposit with thin sand laminae below 1 inch thick. Average net-to-gross is about 6%.

The three facies identified in the 8 reservoir are channel, levee and overbank deposits (labelled A, C and E, respectively, in Fig. 12). The definition of the spatial variation of the facies is challenging, as the typical scale of their distribution is near or below seismic resolution.[7] Furthermore, except where they are cut by channels, the stratigraphic features of the sand are very subtle and difficult to detect on logs since sand response is close to shale response because of the gross intercalation of sand and shale layers whose thicknesses are below the log resolution.[7] The difficulty in identifying the sands from logs is better appreciated by considering their typical appearance as seen on cores (shown in the graphics in Fig. 12).

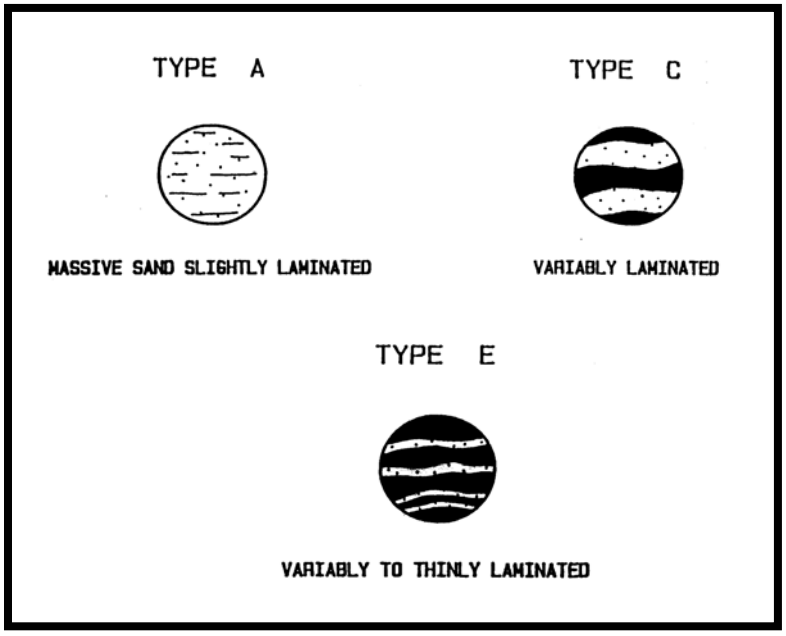

Figure 12: Schematic of facies appearance on core plugs (after Plantevin).[7]

Core study was based on one set of core pictures from well 7. The available pictures were for the interval between 9,961 ftMD and 10,050 ftMD. The most common facies is the levee deposit, which appears as a thinly interbedded deposit consisting of thin beds of well-sorted, very fine-grained sandstone and mudstone. The contacts between sand and shale layers are usually sharp, without any erosion features. Fig. 13 portrays these sand/shale laminations.

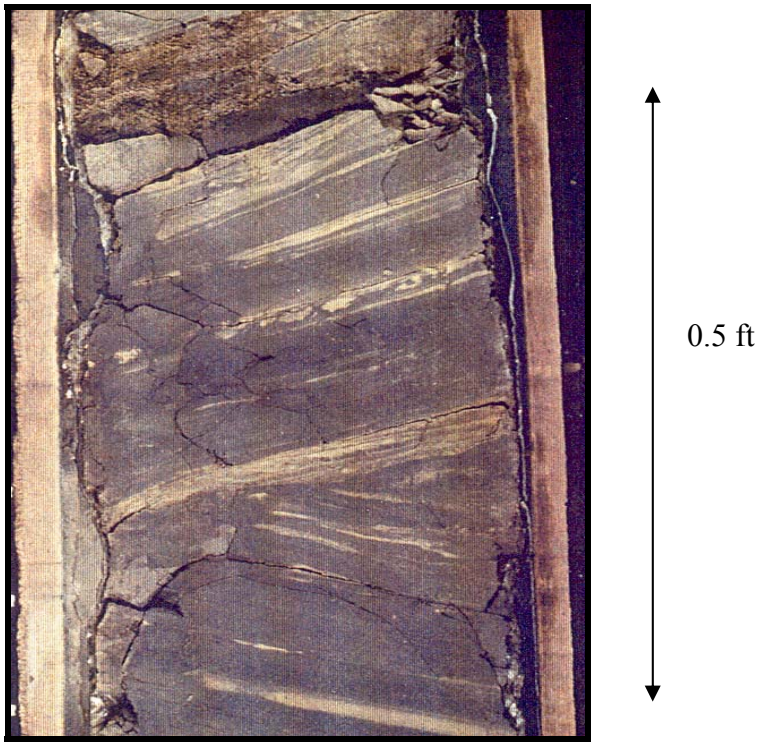

Fig. 13: Core picture showing an angular discordance caused by core twisting in facies E. This core comes from well 7, at a depth of 9,994 ftMD (after Plantevin).[7]

In Fig. 14 observe that the individual sand layers show a thickness range of 0.1-3 inches, although locally sand beds up to one foot thick are present. We interpreted these thickness variations as an indicator of the position of the deposit with respect to the channel location. We assumed a channel cut-off of 2 ft. Therefore the reservoir sand encountered in well 7 was mostly levee deposits with indication of the presence of some overbank deposits. The sand content was computed by measuring the thickness of the sandstone and mudstone layers, and was mostly in the range of 30-70%. In some cores we could detect some fining-upward trends. The sands are either parallel laminated, or display asymmetrical ripple cross-lamination (Fig. 15).

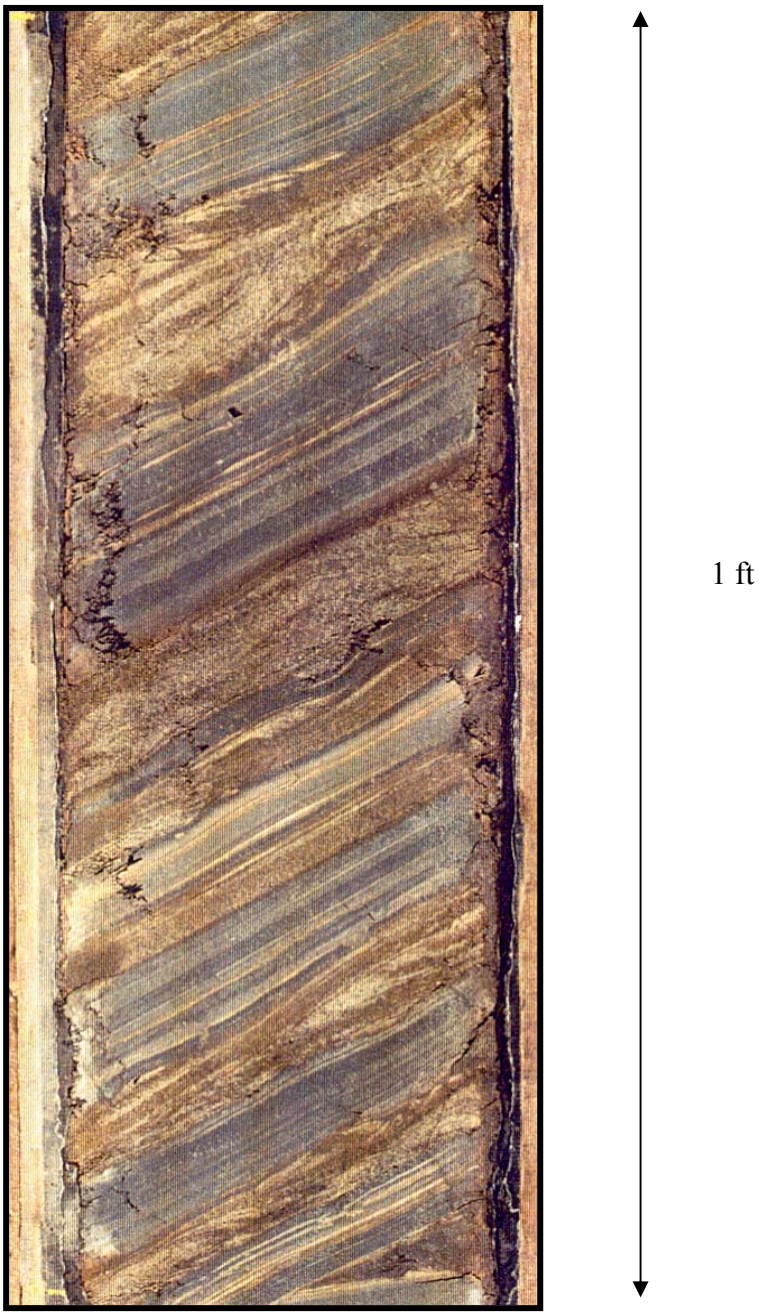

Fig. 14: Core picture showing alternating sand and shale layers in a levee deposit (facies C). This core is taken from well 7, at a depth of 10,034 ftMD (after Plantevin).[7]

Fig. 15: Core picture showing cross ripple lamination in a sand layer. The relatively coarser sand is indicative of a deposit close to a turbidite channel. This core was taken from well 7, at a depth of 10,036 ftMD (after Plantevin).[7]

Because the thickness of the larger sand layer did not exceed 2 feet, the geologist[7] concluded that no channel-fill deposits were visible on the core pictures shown in Figs. 13 through 16, even if at some locations of the interval the deposits are likely to be adjacent to a channel. We also inferred that the vertical permeability inside the reservoir should be very low, regarding the laminated nature of the deposits. Shale interface between channel and levee facies may possibly constitute a flow barrier. Though we cannot infer lateral continuity of the sand/shale strata, it is typical of levee and overbank deposits to exhibit good lateral continuity.

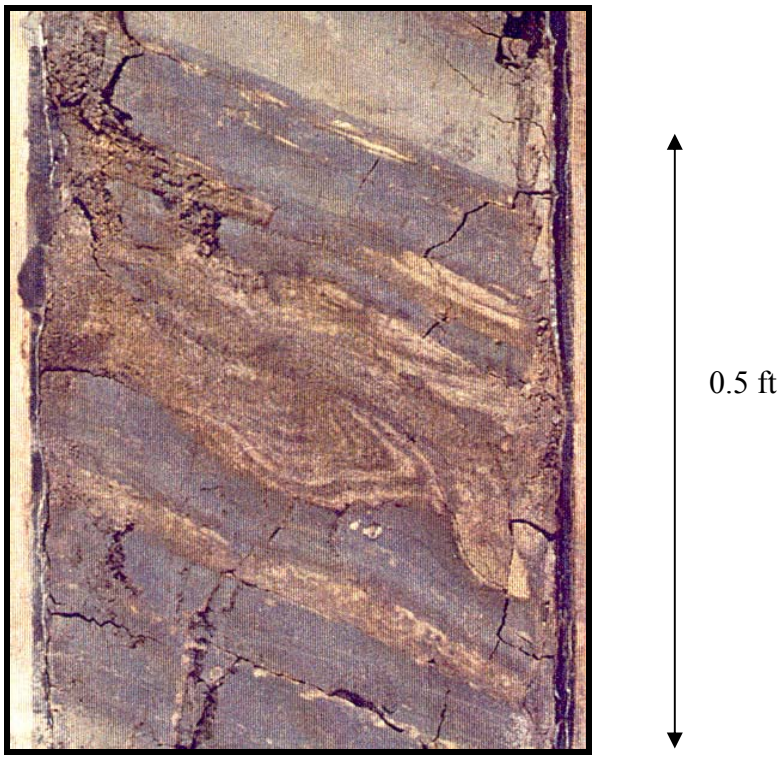

Fig. 16: Core picture showing convolute bedding. This core was taken from well 7, at a depth of 9,966 ftMD These structures point to conditions of rapid deposition. Some portions of the core contained more mudstone facies, indicating a deposition further from the channel (after Plantevin).[7]

Porosity

In general, reservoir quality in individual sand layers is high, with porosities around 35% and permeabilities that can reach 3300 md. One of the main features in the cores is that the sediments are unconsolidated because diagenetic modification of depositional porosity and permeability is minimal. Thus reservoir quality is controlled principally by depositional facies.[15]

Fig. 17 is a crossplot of log-derived porosity against core-derived porosity. As we see, log porosity correlates well with core porosity. The overbank deposit exhibits a well-defined trend of direct proportionality between the log of permeability and porosity. The levee deposit also shows a not-so-well-defined trend, but the channel deposit does not show the expected direct proportionality.

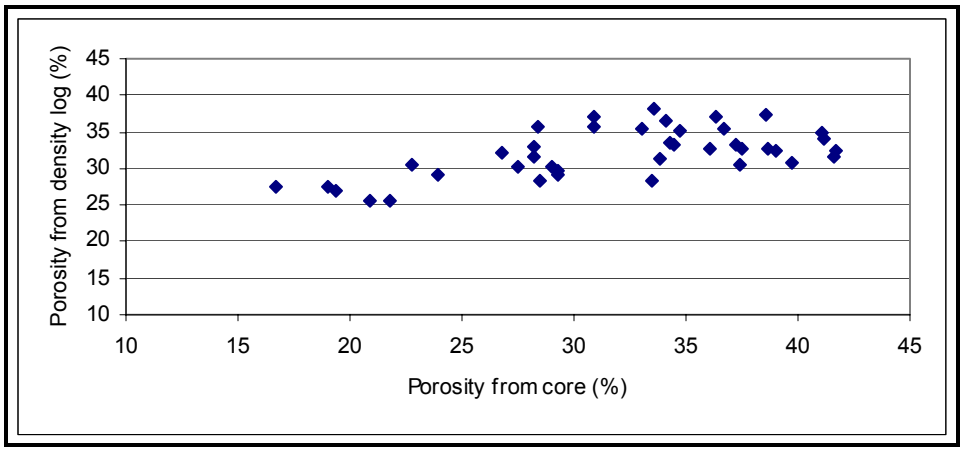

Fig. 17: Correlation between porosity values from cores and from logs (after Plantevin[7])

Connate Water Saturation

Because the more populous values of connate water saturation, S_{wc}, determined from resistivity logs compared well with those obtained from core analysis, those determined from logs were used. Fig. 18 is a cross-plot of water saturation against porosity. Since porosity is facies-dependent, connate water saturation is therefore facies-dependent. The figure shows an inverse relationship between the S_{wc} and the porosity. This may infer that the reservoir sand is clean as the presence of contaminant minerals (e.g., illites) would becloud the correlation and obliterate the trend.

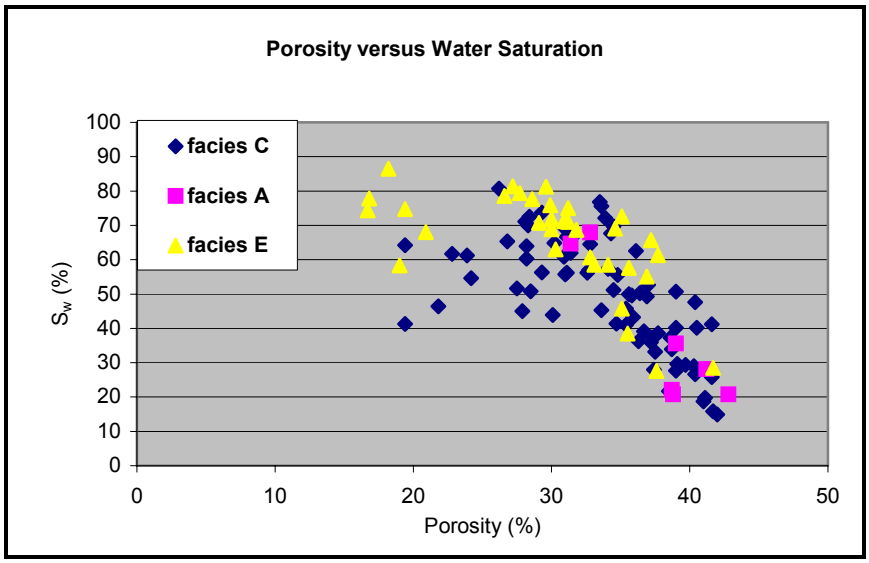

Fig. 18: Correlation between water saturation and porosity - from cores and from logs (after Plantevin).[7]

Gross and Net Thicknesses

Table 2 shows the results of the reservoir thickness interpreted from logs. The combination of these results and seismic data yielded the gross and net thickness maps. The net-to-gross ratio is derived from the gross and net thickness values.[6,7]

Table 2: 8 sand interval gross thickness, net thickness and net-to-gross ratio (after Plantevin[7]).

Well	Gross thickness (ft)	Net thickness (ft)	Net-to-gross (%)
1	72	35	48.6
2	154	76.5	49.7
3	146	72.5	49.7
5	35	14.8	42.3
7	126	58.7	46.6
7st	126	54.3	43.1
8	53	26	49.1
11	71	30	42.2
12	89	35	40
12st	130	52	40
25	121	59	48.8

Net-to-gross ratio varies from 30-50% in the proximal levees to 10% in the distal overbank.[10] The log response in the levee and overbank facies, commonly called "low pay, low resistivity sands," is highly variable and is generally described as nervous or ratty.[7] The thin sand/shale laminations, on the order of a few inches, significantly hinders log interpretation due to the attenuation of the log response by the intercalating shales. The presence of channels is portrayed by the pronounced excursions of the log signature from the shale base line. Table 3 summarizes the results of the interpretations of the logs run in the wells that traversed the 8 reservoir, showing the various facies and their corresponding porosities and permeabilities.

Table 3: Vertical distribution of facies per well used to populate the 8 reservoir rock (after Plantevin).[7]

Well	Depth MD	Facies	Kair (mD)	Por (%)	Well	Depth MD	Facies	Kair (mD)	Por (%)
A-11	9981	B	225	29	**A-7**	9963	B	302	35
	9985	E	2	18		9964	A	338	39
	10020	C	200	29		9965	A		39
	10025	C	800	34		9965	C	618	37
	10030	C	860	33		9976	C		40
A-12	11890	C	234	37		9977	C		42
	11890	C	153	35		9978			39
	11891	C	645	39		9979	C		40
	11894	C	710	36		9989	C	166	39

Well	Depth MD	Facies	Kair (mD)	Por (%)
A-12	11894	C	650	39
	11895	C	106	28
	11896	C	89	31
	11896	C	62	26
	11897	C	233	35
	11898	C	195	31
	11900	C	95	33
	11901	C	314	37
	11902	E	151	31
	11904	E	109	28
	11907	E	257	38
	11908	E	185	30
	11909	E	124	29
	11910	E	109	27
	11911	E	187	29
	11915	E	260	35
	11918	E	328	30
	11919	E	200	31
	11920	E	303	35
	11922	E	186	31
	11922	E	360	34
	11923	E	428	37
	11924	E	178	33
	11925	E	176	36
	11926	E	672	42
	11927	E	205	30
	11928	E	403	36
	11928	E	239	32
	11929	E	132	33
	11929	C	754	35
	11930	C	340	35
	11931	C	309	37
	11932	C	499	38
	11933	C	661	33
	11934	C	596	36
	11935	C	697	39
	11937	C	193	31
	11938	C	706	28
	11939	C	412	34
	11940	C	163	32
	11941	C	596	35
A-27	12353		1	18
	12377		1	18
	12388		16	22

Well	Depth MD	Facies	Kair (mD)	Por (%)
	9993	C		29
	9997	B	514	40
	9998	A		39
	9998	A	516	43
	10002	A	173	41
	10002		45	36
	10003	C	108	36
	10005	C	352	38
	10007	C	195	37
	10010	C	44	37
	10012	C	56	34
	10014	C	294	41
	10023	C	139	39
	10024	C	213	41
	10028	C	816	41
	10036	C	371	42
	10037	C	488	40
	10046	C	125	36
	10048	C	41	34
	10049	C	541	40
	10051	C	626	42
A-8	12590	C	104	29
	12601	E	1	17
	12605	C	155	28
	12607	C	195	24
	12613	C	190	28
	12615	C	175	28
	12617	E	5	17
	12619	C	98	23
	12621	C	840	34
	12623	C	630	28
	12625	E	11	19
	12627	C	215	27
	12635	C	280	31
	12644	E	18	19
	12650	C	36	22
	12658	E	13	21
A-25	9897	C	35	24
	9917	C	890	30
	9949	C	210	31
	9961	C	450	30
	9979	A	2100	31
	9984	C	80	28
	9992	A	2600	33

Geology and Geophysics

Two lateral zones with different average properties were delineated using net thickness values derived from log and seismic data.[15] Three facies, channel, levee and overbank deposits, (marked as A, C, and E, respectively) were identified based on petrophysical interpretations. In modelling the reservoir, it was assumed that reservoir heterogeneity is determined by the facies distribution.[7]

The many layers constituting this turbidite system are levee and overbank deposits that are expectedly associated with channel systems. The channel fill commonly appears to be massive, being comprised of

amalgamated sandstones. The coarsest and thickest deposits are levee sands which occur proximal to the channel margin, whereas the mud-rich, lenticular-bedded sequences are found in the more distal overbank sites.[11] The levee and overbank deposits, which consist of alternating sands and shales, are also known as low-resistivity, low-contrast, thin-bedded sandstones.[14] The reason is that, though the individual layers can be excellent reservoirs because of their high porosities and permeabilities,[16] they are so thin that they are below the traditional electrical logging tool resolution.

Structure

The 8 reservoir structure is a north-northwest-plunging anticline bounded to the south by a northwest-southeast trending, southwest dipping salt-detachment fault (Fig. 6). The main features of the field are a salt-induced geometry and the fault system. The northward plunge of the structure (Fig. 19) is opposite the regional basin southerly paleo-dip as a result of salt tectonic activities to the south.[6] The 8 reservoir being simulated is almost trapezoidal when viewed from the top with the NW-SE striking fault bounding the southern end (Fig. 19). The crest of the structure is located along the fault.[11]

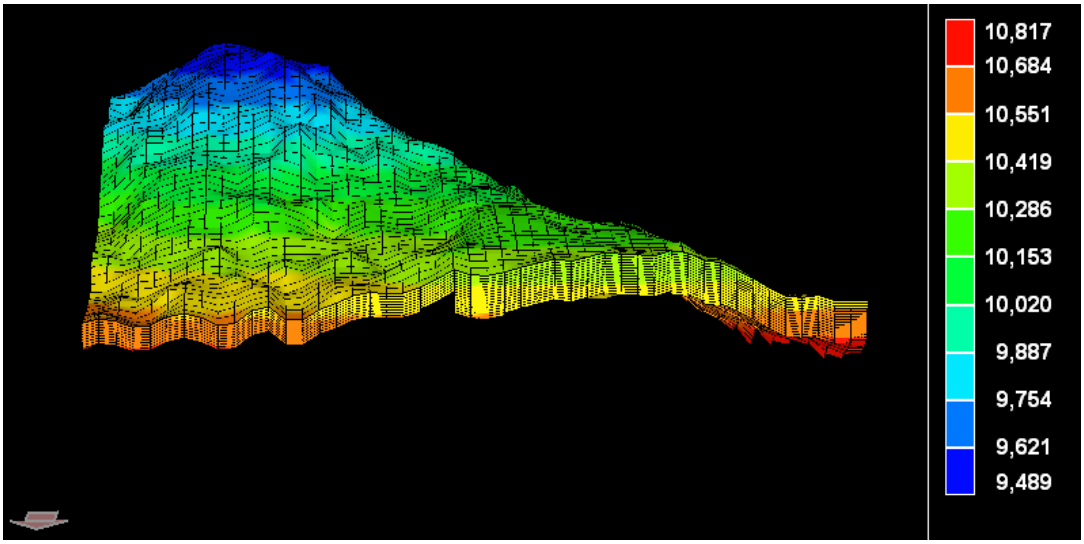

Fig. 19: Southward 3D view of the 8 reservoir structure.

Stratigraphy

The stratigraphy of the reservoir was determined from interpretation of log and core data. The results of these interpretations at the well locations formed the pilot (or master) points for a distribution of the facies using geostatistics. Figs. 20, 21 and 22 are structural cross sections derived from log and core data. Their locations are indicated in Fig. 23. Channels may not have been properly located on the cross-sections

shown. The cross-sections indicate that dominant facies are levee and overbank deposits; channels are sparse.

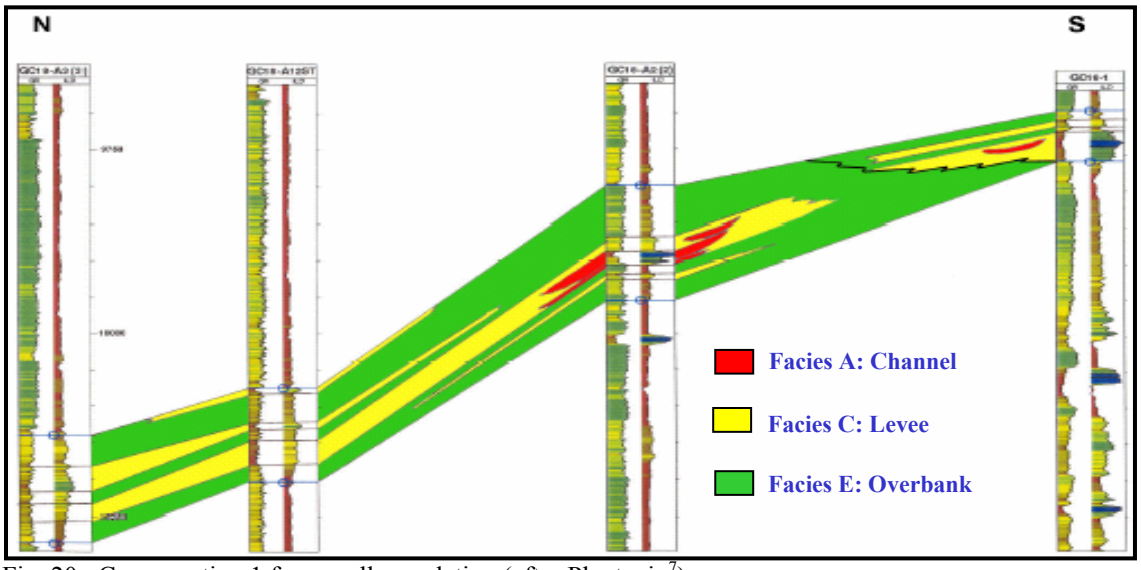

Fig. 20: Cross-section 1 from well correlation (after Plantevin[7]).

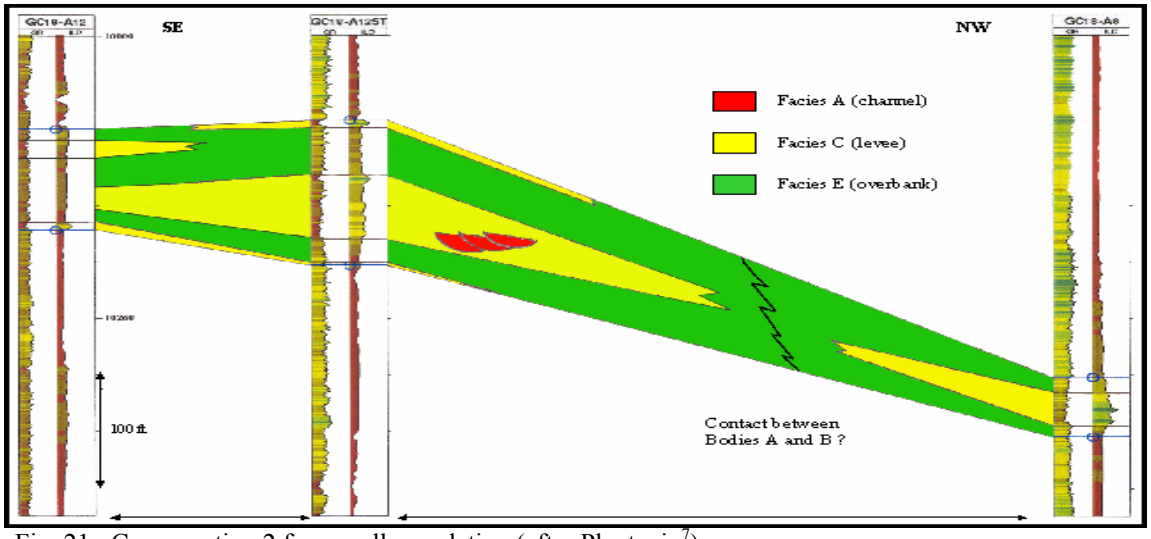

Fig. 21: Cross-section 2 from well correlation (after Plantevin[7]).

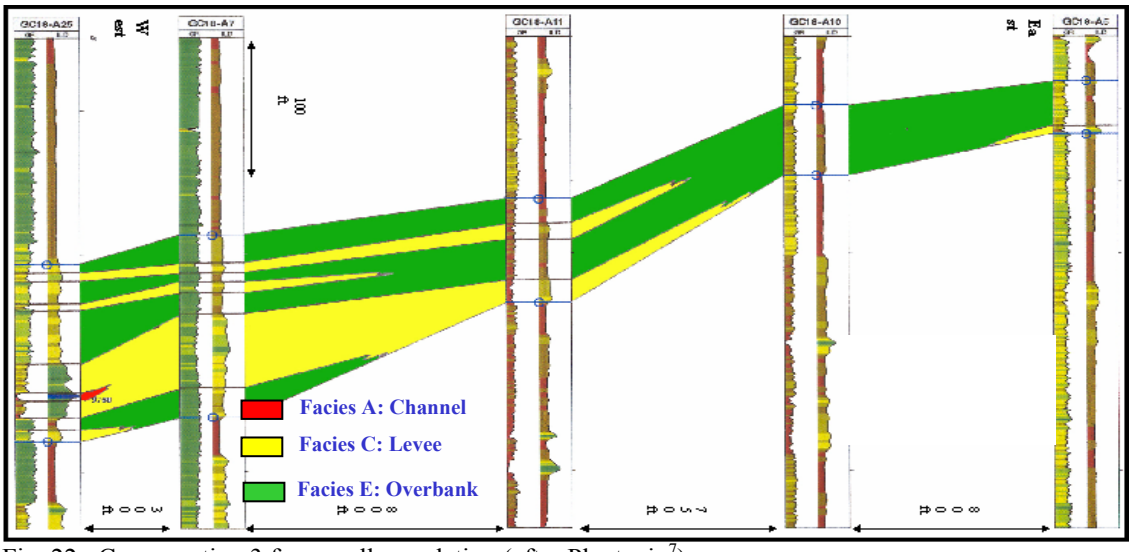

Fig. 22: Cross-section 3 from well correlation (after Plantevin[7]).

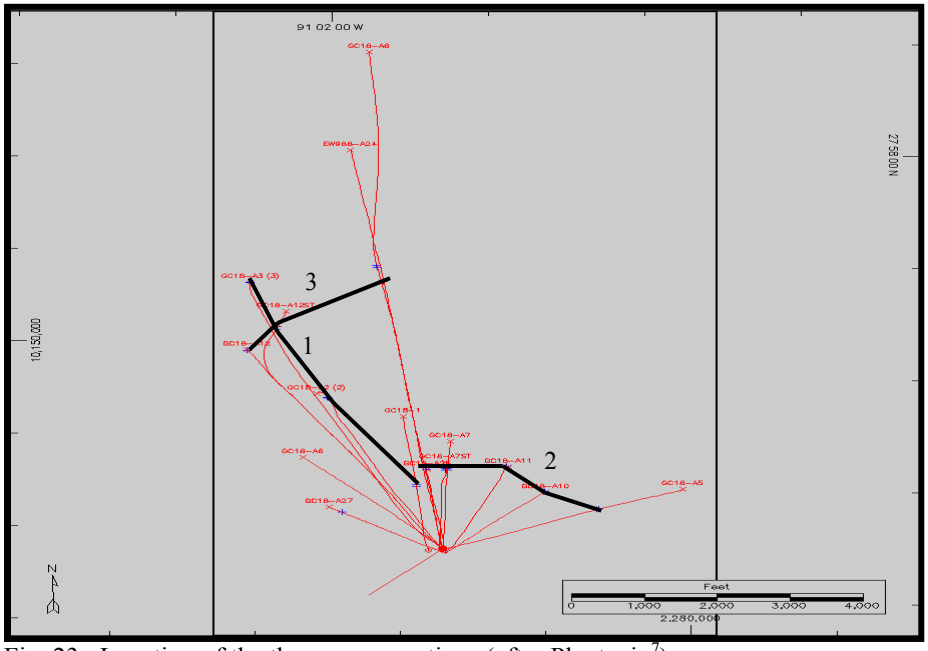

Fig. 23: Location of the three cross-sections (after Plantevin[7]).

Permeability Determination

A porosity-versus-permeability cross-plot, based on core data, was used to determine permeability values (Fig. 24). The permeability is generally good for all the facies. Permeability and porosity are well

correlated for the overbank deposit (facies E), but the relationship is less developed for channel and levee deposits (facies C and A).

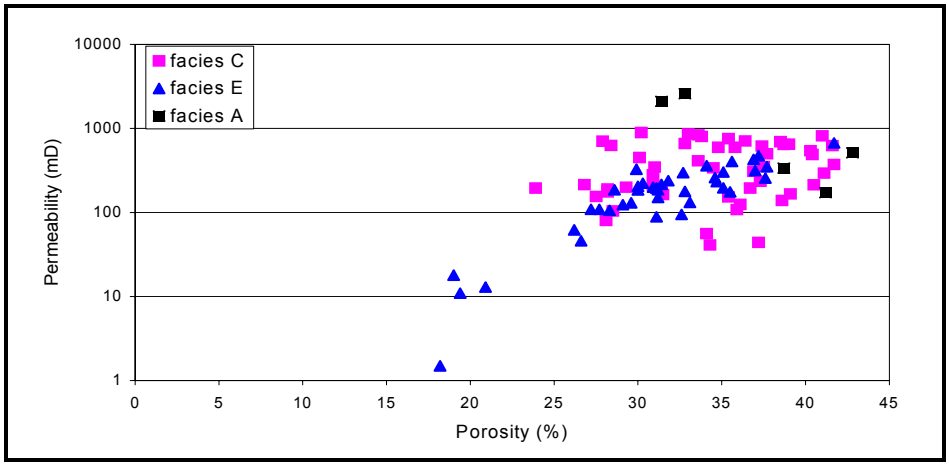

Figure 24: Plot showing permeability vs porosity relationship of facies A, C and E (after Plantevin).[7]

Relative Permeability and Capillary Pressure Data

Relative permeability and capillary pressure data were determined from the "Special Core Analysis," SCAL, performed on the cores from well 7 by Core Laboratories, Inc., in December 1989,[17] and by Petroleum Testing Services, Inc. in mid-1987.[18]

The Amott wettability test was used to determine the connate water saturation, which ranged from 34% to 57%. The residual oil saturation in an imbibition displacement process was determined to range from 20% to 37%. Porosity ranged from 17% to 43%. These values do not only exhibit a wider range, but the upper limit is also considerably higher than log-derived porosity values.

Capillary pressure was determined through the mercury injection capillary pressure experiment performed on six samples with air as the wetting phase. Table 4 contains the end-point relative permeability and capillary pressure data used in this study. Figs. 25 and 26 show the average relative permeability, while Figs. 27 and 28 show the capillary pressure curves used in this study.

Relative permeability data were determined from steady-state relative permeability tests performed on five samples. Two sets of experiments were performed, consisting of one with water as the driving fluid and another with gas as the driving fluid.

The SCAL also provided the rock compressibility from experiment to be circa 27.0E-6 psi^{-1} for a normally pressured rock of the average 30% porosity obtained in the 8 reservoir. Accounting for the effect of overpressure, we have used the obtained value as our minimum and sensitized on higher values.

Table 4: End-point relative permeability and capillary pressure data used.

S_w (%)	k_{rw}	k_{row}	p_c (psi)
80	0.2	0	1.1
25	0	0.9	10.5

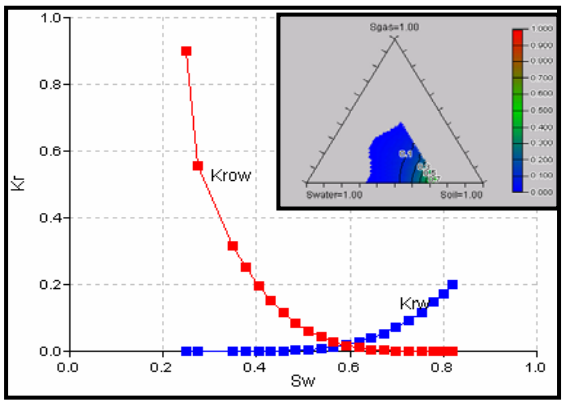

Fig. 25: Oil and water relative permeability curves (red = k_{row}; blue = k_{rw}). Inset is the 3 phase relative permeability representation.

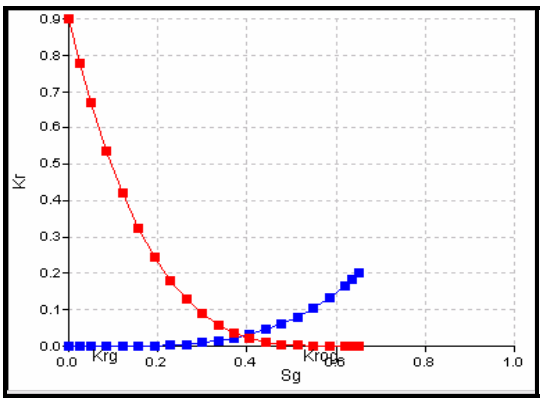

Fig. 26: Gas and oil relative permeability curves (red = k_{rg}; blue = k_{rog}).

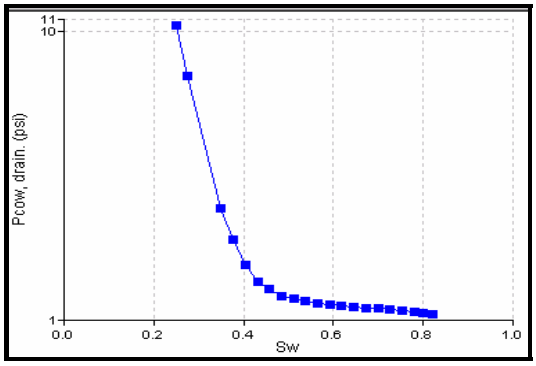

Fig. 27: Oil drainage capillary pressure curve: P_{cow} vs S_w.

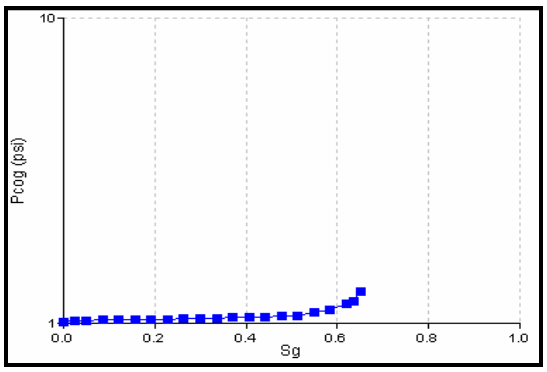

Fig. 28: Oil to gas capillary pressure curve: P_{cog} vs S_g.

PVT Data

Fluid properties used were determined from laboratory experiments. Analysis of the chemical and physical characteristics of a recombined surface sample was carried out by Weatherly Laboratories, Inc.[19] As the sample was taken in well 3, about one month after the reservoir came on stream, it is considered to be representative of the original reservoir fluid. The laboratory evaluation of the fluid showed the 8 reservoir oil to be undersaturated at its initial pressure of 7910 psia. A bubble point pressure of 7750 psia was determined. Table 5 shows the key PVT data used in this study. Figs. 29 through 33 portray the behavior of key PVT parameters with pressure.

Table 5: Key PVT parameters used.

R_{si} (scf/stb)	B_{oi} (rb/stb)	c_o (1/psi)	T_{res} (^oF)	p_i (psia)	p_b (psia)
1,323	1.533	7.9e-6	174	7,910	7,750

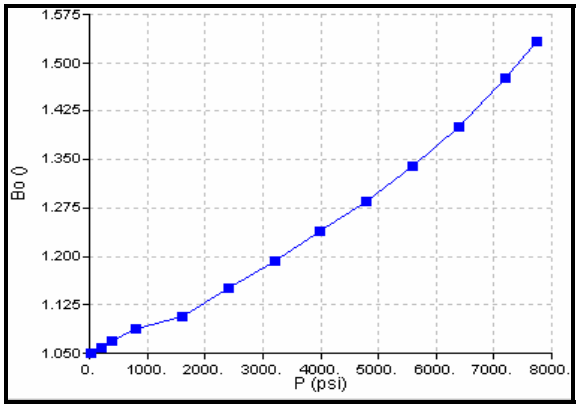

Fig. 29: Formation volume factor, B_o, vs pressure.

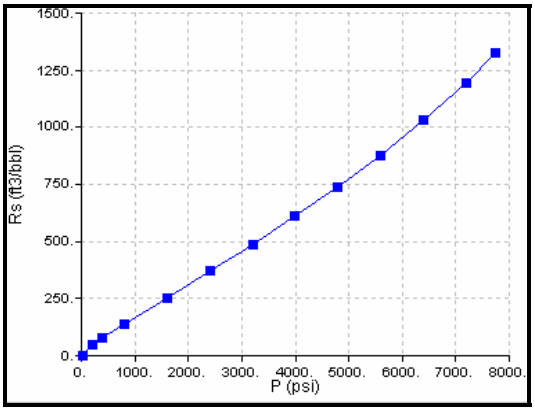

Fig. 30: Solution gas-oil ratio, R_s, vs pressure.

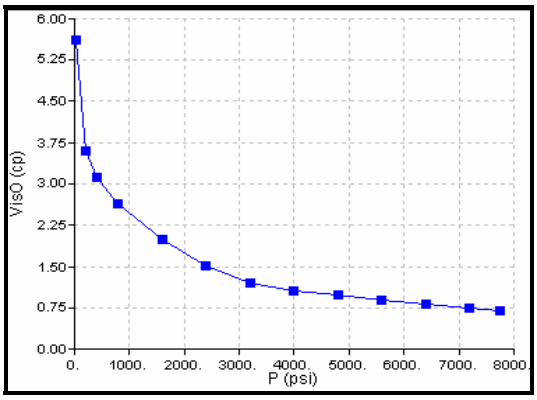

Fig. 31: Oil viscosity behavior with pressure.

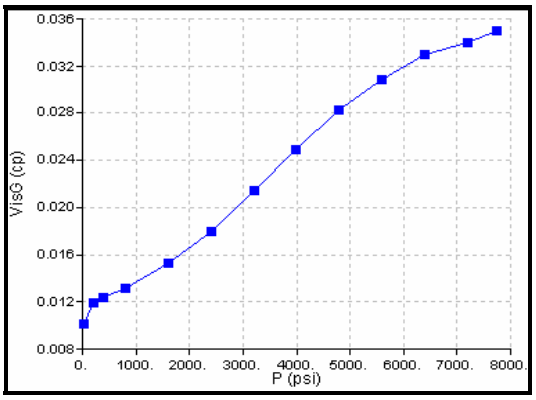

Fig. 32: Gas viscosity profile with pressure.

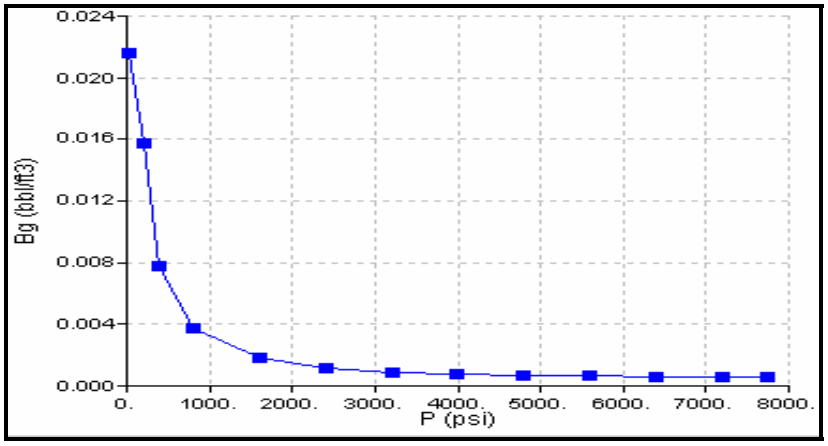

Figure 33: Gas formation volume factor, B_g, behavior with pressure.

Production and Pressure History Data

Production rate data for the reservoir are available for oil, water and gas from first oil in December 1987 until August 2001. Cumulative oil production from this field is about 8.2 mmstb, representing some 34.1% of its STOIIP of 19.8 mmstb. Only monthly production rates are available. Available pressure data are from the four wells 3, 12, 6, and 7, and terminate in August 1998. Build-up periods for these bottom-hole pressures range from 4 hours to 24 hours.[5]

Oil Production Data

Figs. 34 and 35 portray the oil and water production history of this reservoir. Initial hydrocarbon withdrawal was from the two wells 3 and 12 in the western region of the reservoir. The reservoir production quickly rose to an initial peak of ca 2,200 bopd, and then commenced a steady decline, reaching

a low of ca 400 bopd in December 1993, and then, through possible human intervention, rose slightly to ca 500 bopd. However, with the coming on stream of the wells in the eastern region in June 1996, the reservoir enjoyed a boost in its production to an all time peak of ca 5,300 bopd. But the decline that followed this was very steep as only well 6 was responsible for this prolific performance. However, the rate increased from ca 2,000 bopd to ca 4,500 bopd with the recompletion in December 1998 of well 2 in this reservoir. The recompletion of well 9 in this horizon in November 2000 contributed only marginally to the total production and only marginally offset the persistent decline, which has continued to date.

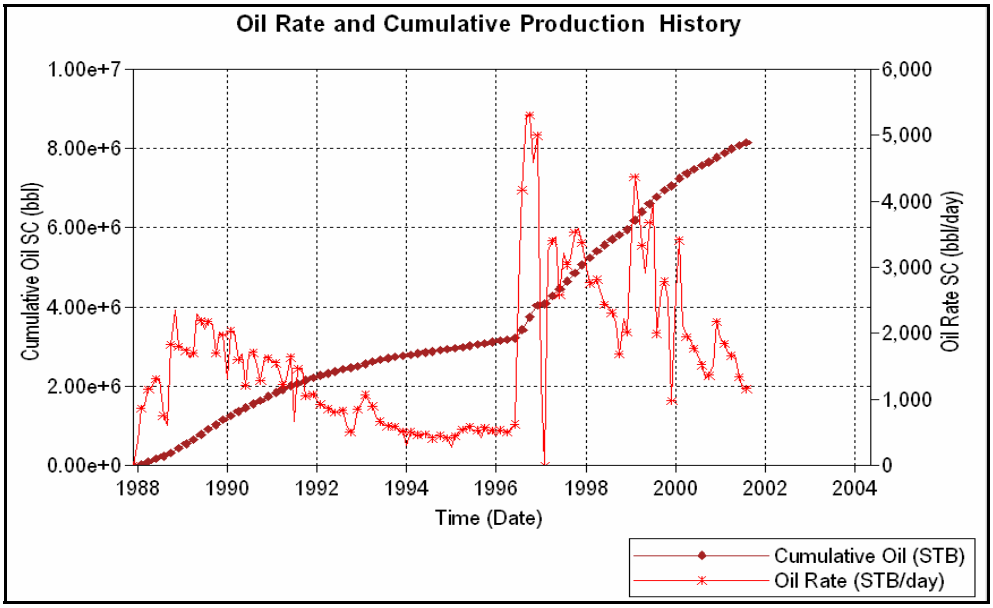

Fig. 34: Observed 8 reservoir oil rate and cumulative production history plot.

Water-Cut Data

Field water-cut, shown in Fig. 35, rose to its maximum of 66% in June 1996. It experiences a significant drop to ca 17% with the coming on stream of prolific well 6. It soon resumes a steady climb and reaches ca 53% in December 1999. However, the significant contribution to the oil rate by well 2 causes another drop in the water-cut to ca 21%. It soon resumed its climb and as of 09/2001 is at ca 40%.

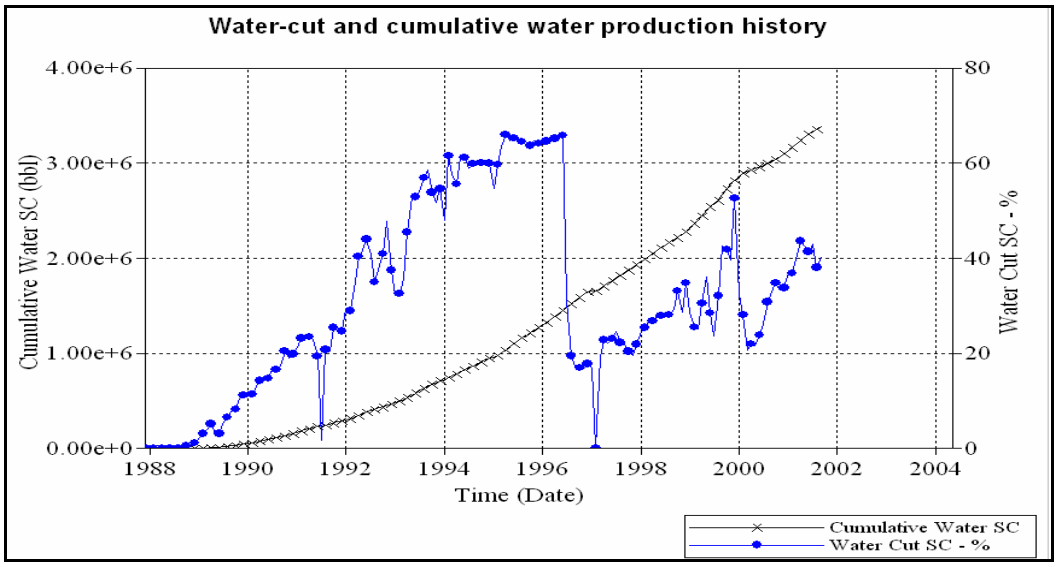

Fig. 35: Observed 8 reservoir water-cut and cumulative water production history.

Gas-Oil Ratio Data

Producing gas to oil ratios (GOR) remained approximately steady at ca 900 scf/stb for about 1 year then rose quickly to over 1,200 scf/stb. Fig. 36 portrays the history of the 8 reservoir.

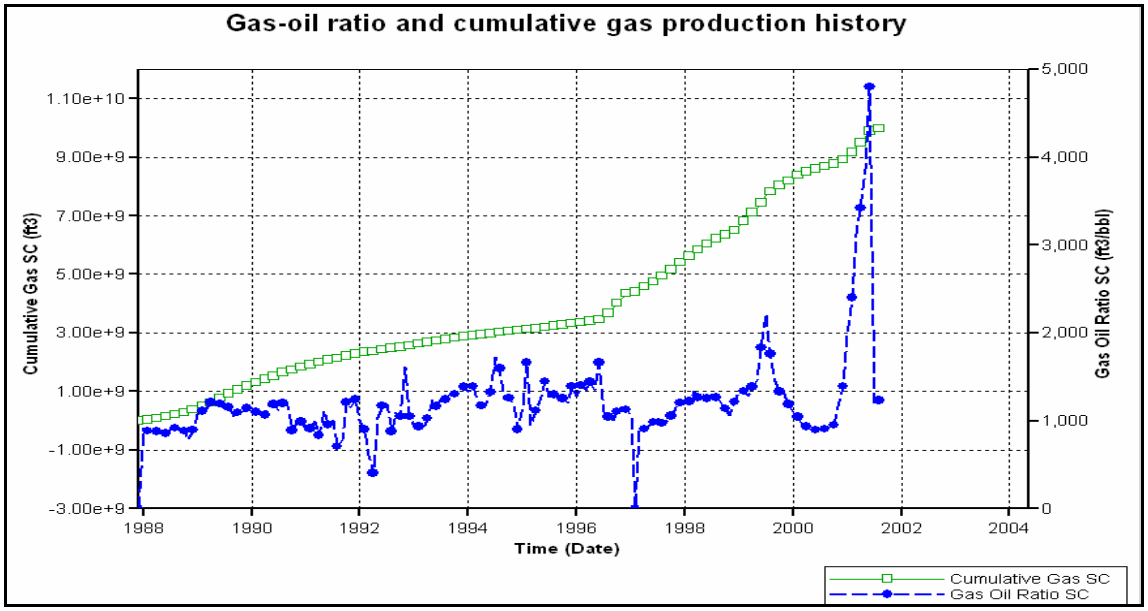

Fig. 36: Gas-oil ratio and cumulative gas production history.

Production Data from Wells

Production from the 8 reservoir has been from seven wells, namely wells 2, 3, 6, 7, 9, 12, and 25. Production from the reservoir started from well 3 in December 1987. Production from this well peaked at ca 1800 bopd about a year after first oil, but began a steady decline almost immediately upon reaching this peak.

Well 12 came on stream some 10 months after well 3. Production from this well peaked some 10 months later at ca 1000 bopd. Like well 3, the production from this well began a steady decline almost immediately after it reached its peak. Fig. 37 shows the oil production rate history of wells 3 and 12.

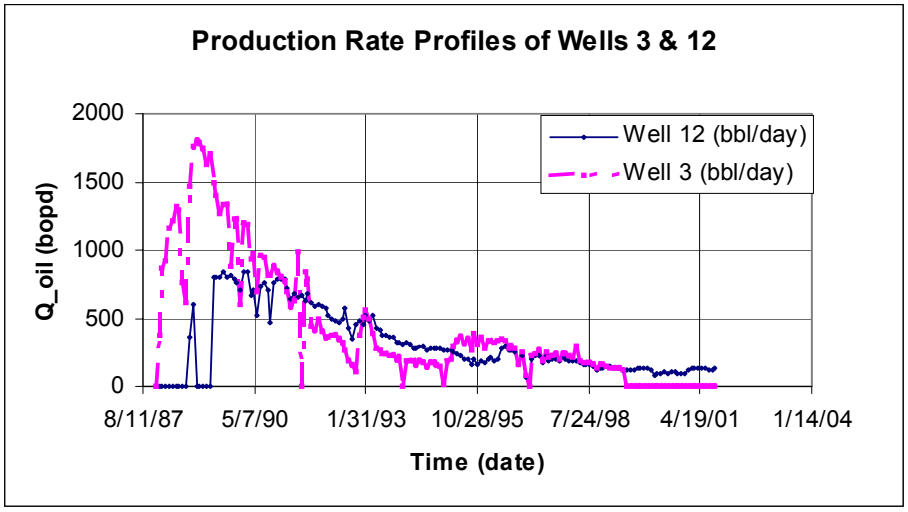

Fig. 37: Oil production rate profiles of wells 3 and 12.

Withdrawal from the reservoir was greatly boosted by mid-1996 when wells 6 and 7 were brought on stream in quick succession. Well 6 proved to be a prolific producer, quickly reaching its peak of over 3600 bopd a few months after coming on stream, and reaching a cumulative oil production of ca 2.636 mmstb about 3.7 years after coming on stream.

Well-7 lived a very brief production life. It produced very poorly and was plagued by high water-cut.

First oil from well 2 occurred in 01/1999. However, the well was shut in some 6 months later for about 6 months. It came back into production in 12/1999 and produced outstandingly, such that in 31 months, its cumulative production topped 1.34 mmstb oil. The well contributed significantly to the total recovery from the 8 reservoir. Like other wells in this region, water breakthrough occurred early in its two producing periods. Each time the water-cut rose sharply. Fig. 38 shows the oil production profiles of wells 2, 6 and 7.

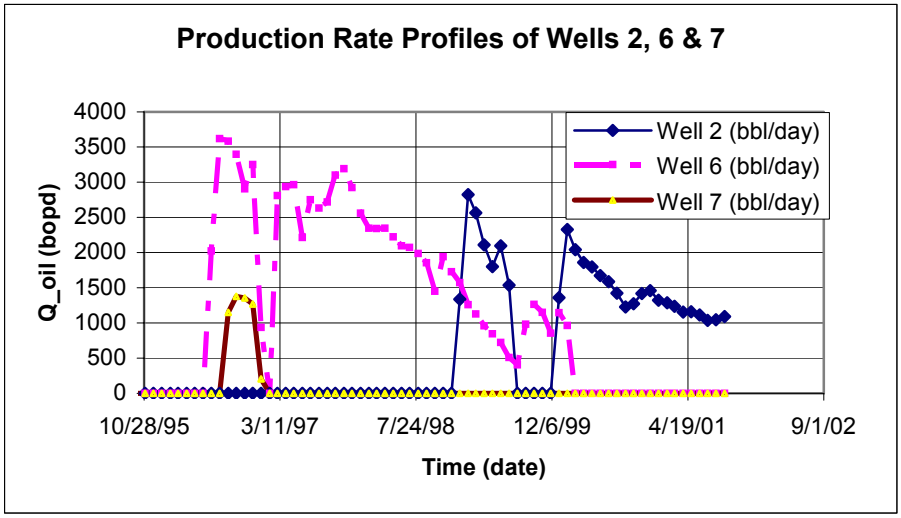

Fig. 38: Oil production profiles of wells 2, 6 and 7.

Pressure Data

Static bottomhole pressure surveys taken in four wells (wells 3, 12, 7 and 6) constitute the pressure data in the 8 reservoir. The available data spans from 01/1988 to 07/1998. The buildup duration ranged from 4 hours to 24 hours.[5] Fig. 39 shows the pressure history of the reservoir.

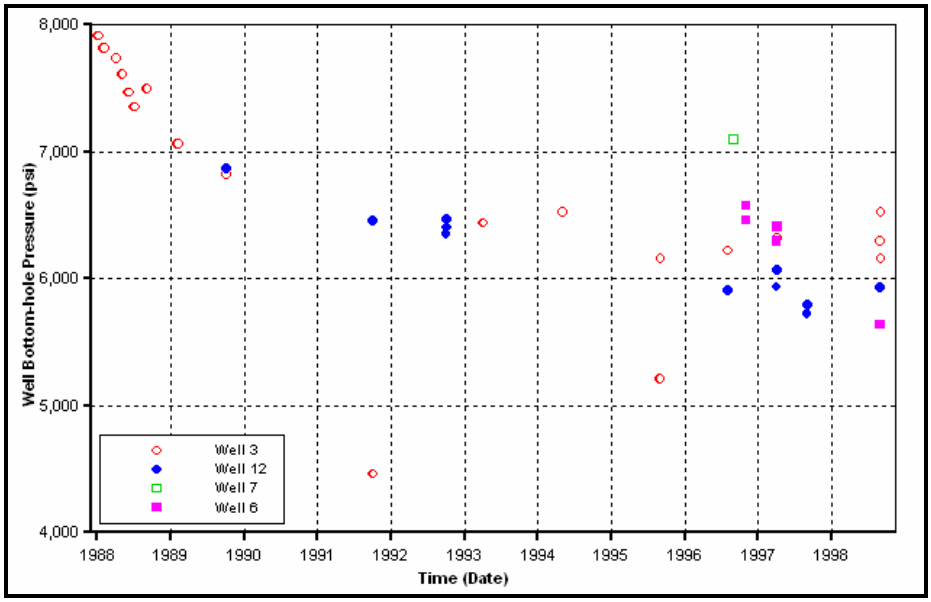

Fig. 39: Pressure history of the 8 reservoir.

Initial Thoughts on the 8 Reservoir Performance

The 8 reservoir is a closed system that became geopressured as a result of post-accumulation rock tectonics, specifically salt tectonics caused by the salt diapir located to the southeastern quadrant of the block. Because the observed pressure behavior is not commensurate with the original overpressure, which has been sustained to a lesser but steady degree over this reservoir's producing life, the source of pressure support constituted a puzzle.

Concerning the source of the observed pressure support, three different schools of thought existed:

One school postulated that pressure support and observed water production resulted from communication of the reservoir with another proximate reservoir above or below it through one of the wells penetrating this reservoir, especially through one of the wells that failed due to rock plastic stresses induced by pressure variations resulting from drilling or production activities.

The second school of thought postulated that the pressure behavior and observed water production was a result of either the expulsion of water by the interlayering shales or the intrusion of the shale itself into the pore spaces of the sand in response to voidage caused by reservoir fluid withdrawal. It argued that, once initiated, whichever of the two mechanisms mentioned above that is at play continued with continued reservoir voidage due to production.

The third school of thought attributed the observed pressure and water production behavior to the reservoir being more extensive than currently captured in the maps, and that it contained a finite water-leg attached to it.

We tested the third school of thought by simulating the 8 reservoir with an extended hydrocarbon accumulation. The results could not match the observed reservoir behavior at any point of the reservoir's producing life.

The second school of thought, which considered the reservoir rock's mechanical response with pressure depletion, first assumed the reservoir rock to be of very high plasticity. Secondly, it assumed real-time voidage replacement by the shale rock intruding into the pore spaces "vacated" by produced fluid, an assumption that further assumes that the shale rock is so plastic it exhibits the reservoir fluid mobility properties. These assumptions are based on extreme behavior of rocks, which may be attainable under extreme conditions of temperature and pressure with associated change in the rock mechanical properties. The required extreme conditions of temperature and pressure do not exist in the 8 reservoir.

On the first postulation, if communication is established through a well that failed due to rock stresses, it is expected that with time, because the rock is unconsolidated, the pathway between the communicating reservoirs will completely heal if it is not held open by the diligence of human intervention in order to counter the natural healing capacity of the unconsolidated rock. I believe that this postulation is likely

invalid, and, even if it were the case, it is feasible that some other factors may also be at work either in concert or in exclusion, and with or without the human interventions alluded to. Put in another way, the chances of the 8 reservoir communicating with another reservoir are slim; some other mechanisms are responsible for the observed reservoir behavior. Other mechanisms were investigated in the model calibration phase of this study.

CHAPTER III

STATIC RESERVOIR CHARACTERIZATION

Framework and Structure

The framework of the 3D geologic model is built on the presence of two major features, faults and salt presence. The reservoir structure was defined by projecting well log data onto seismic interpretation using deviation data. The 8 reservoir was logged in 14 wells. Their locations and TVD's of penetration of the sand served as pilot points for mapping the top of the sand. The gross- and net-sand thicknesses (Figs. 40 and 41) of the sand were determined by tying in seismic frequency and interval velocity with well data. [8,9] Figure 42 is the 3D representation of the reservoir structure.

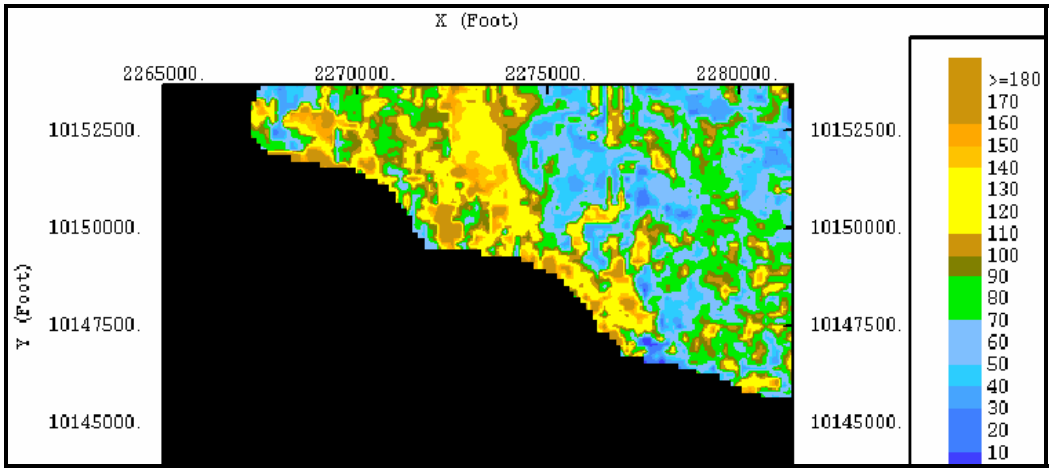

Fig. 40: Gross sand thickness map (after Lalande[6]).

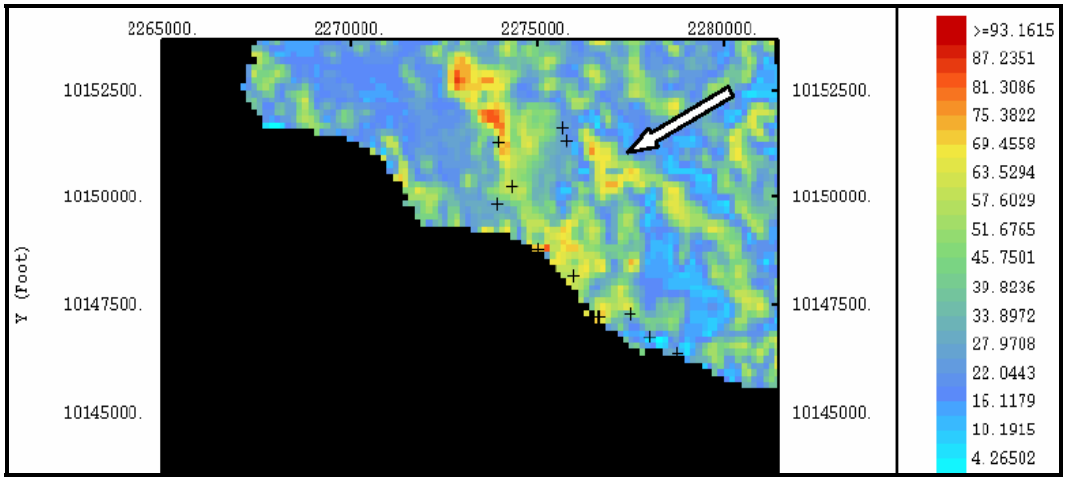

Fig. 41: Net sand thickness map (after Lalande[6]).

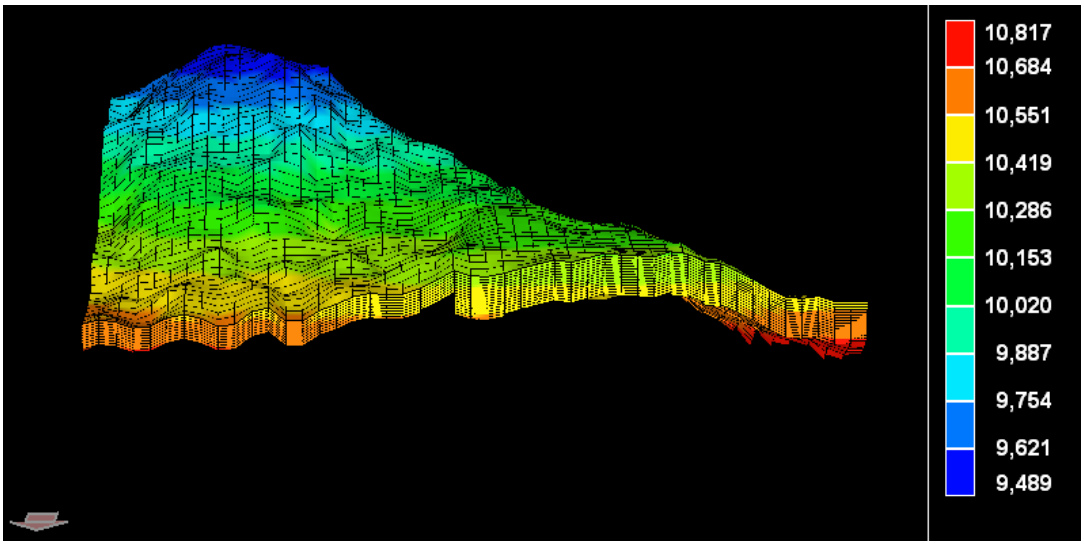

Fig. 42: Southward 3D view of the 8 reservoir structure.

Stratigraphy and Facies Distribution

Two lateral regions with different average properties were delineated using net thickness values derived from log and seismic data. The three facies, channel, levee and overbank deposits, were identified in both regions. The two regions, located in the east and west of the reservoir, were seen to overlap at approximately the mid north-south-oriented line (Figs. 43 and 44) [6,7] in an approximately NNE-SSW trend. The western region has higher overall thickness than the eastern region.

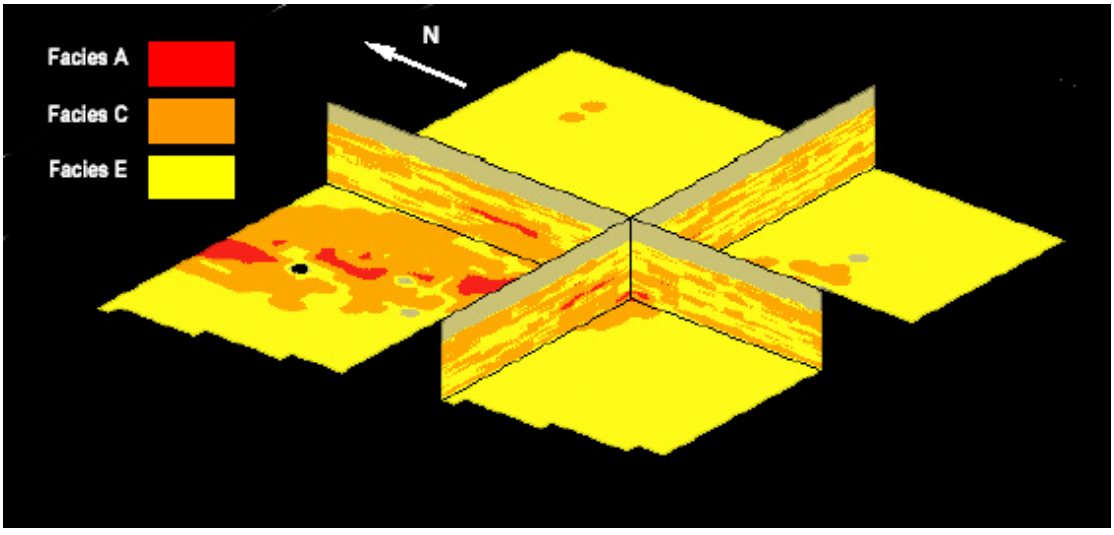

Fig. 43: 3D lithofacies geostatistic simulation of the 8 sand (after Lalande[6]).

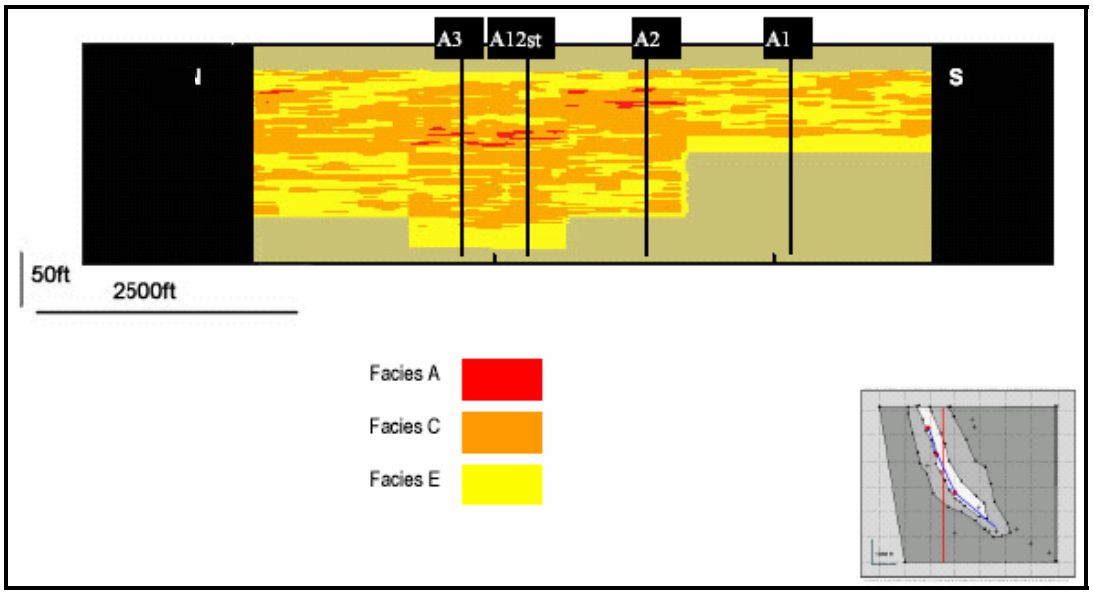

Fig. 44: North-south cross-section of the 8 sand lithofacies distribution (after Lalande[6]).

This study is the first comprehensive integrated reservoir management effort towards quantifying geological parameters and assessing their impact on reservoir performance by using the latest reservoir data from the study area. Different geological realizations were modelled including:

1. A multi-layered reservoir complex with a vertical communication between layers,
2. A multi-layered reservoir complex without vertical communication between layers,
3. A compartmentalized reservoir system in communication with another reservoir, and
4. A vertical and lateral stacking system with multiple distinct facies types.

2D areal maps of the reservoir structure and thicknesses were provided for the first three realizations. Only the fourth realization was provided as a detailed 3D model with the distribution of the different facies. Calibration of the realizations (using history matching) yielded unsatisfactory results for the first three realizations, perhaps due to the coarse geological details. This indicated that a detailed geological characterization was necessary to simulate the 8 reservoir to obtain an acceptable history match. However, the results of calibrating the coarse geologic realizations demanded substantial vertical and lateral heterogeneity, suggesting that the reservoir may be not only vertically stacked as the realizations suggested, but also laterally stacked.

On the strength of the discussion in the paragraph above, we are inclined to conclude that because the fourth realization captured much of the complexity in the reservoir architecture and stratigraphy, it yielded much better calibration results than the rest.

Model Preparation and Initialization

The 3D geological model was created using the geostatistical software ISATIS, and was presented for simulation in a flattened XYZ nodal ASCII format. The fine-grid geologic model contained 95 x 55 x 195 nodes in the X, Y, and Z directions, respectively. The inter-nodal distances were 150 x 150 x 1 ft in the X, Y, and Z directions, respectively. This fine-grid nodal model had facies distributions that were derived from geostatistical simulation. We assigned properties to each facies according to log and core evaluations.

Model Evaluation and Preparation

Because the dynamic simulator (CMG – IMEX[20]) would not accept the 3D model in the format it was presented, intermediate software was used to interface between the geostatistical software and the reservoir simulator. Integrated and geologically oriented computer aided design software, GOCAD[21], was employed for this purpose. With the capabilities of GOCAD to integrate isolated sources like seismic, production data, and geostatistical simulations and unite them in a single 3D environment, we were able to retain the different facies distributions in the 3D model and assign values of properties to each facies.

Two scripts were used to convert the XYZ format to a format acceptable to GOCAD and to assign petrophysical and rock properties to the facies.

Upscaling and Uploading

Single values of the properties of porosity, permeability (in X, Y, and Z directions), and net-to-gross ratio were assigned to each of the three facies modelled in the dynamic simulation. The fine-grid system with the associated facies properties was then upscaled to 47 x 55 x 16 grid blocks in the X, Y, and Z directions, respectively, giving a total of 41,360 grid-blocks (Fig. 45). Of these, 24,177 grid-blocks are void blocks, without properties because they fall on the southern side of the major synthetic fault. Volume averaged upscaling was used on the volume-related properties like porosity, water saturation, and net-to-gross ratio. Permeability, which is a vector quantity, was upscaled as a diagonal tensor.

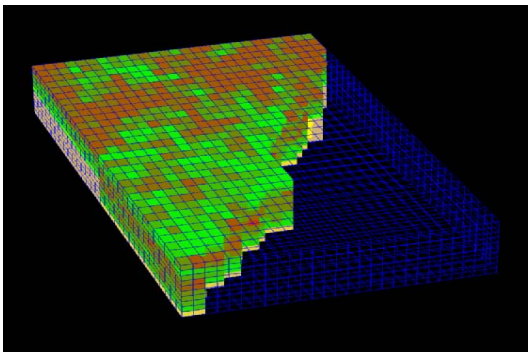

Fig. 45: The detailed 3D model after being upscaled in GOCAD (still flattened)

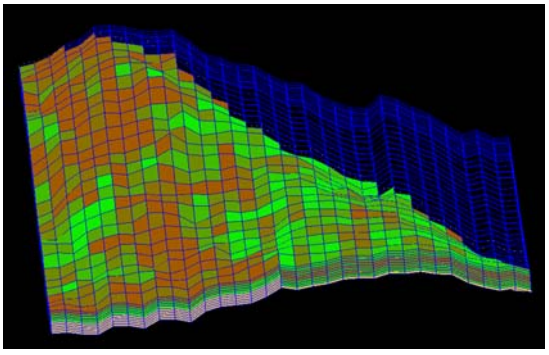

Fig. 46: The upscaled 3D model after being deformed to reservoir topography in GOCAD

The entire XYZ stratigraphic grid-box was then deformed to assume the topography of the reservoir top and bottom (Fig. 46). The resulting 3D coarse-grid static reservoir model was then exported to CMG directly from GOCAD. However, in CMG, the facies lost their individual identity but their associated properties were preserved for the respective grid-blocks where the facies existed. This allows for the facies to still be inferred. The void grids had to be nullified in CMG using an in-built script capability which facilitated the process by allowing all grid-blocks with porosity less than or equal to zero to be nullified. Production and PVT data were subsequently loaded in CMG.

In CMG the model was initialised. Figs. 47 through 49 show the final net-to-gross ratio, porosity, and permeability distributions of the calibrated static model used for dynamic simulation. Fig. 50 is the oil saturation distribution of the final static model used for simulation.

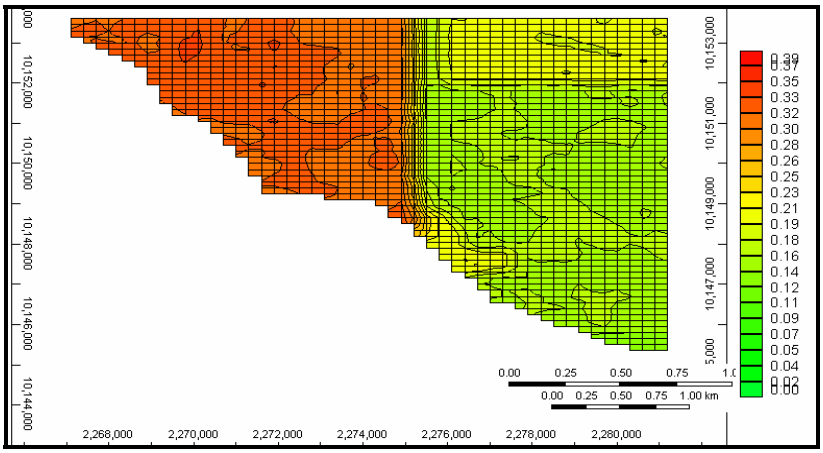

Fig. 47: Net-to-gross ratio map (shown for the 4th layer to illustrate the presence of the overlap in the middle of the reservoir).

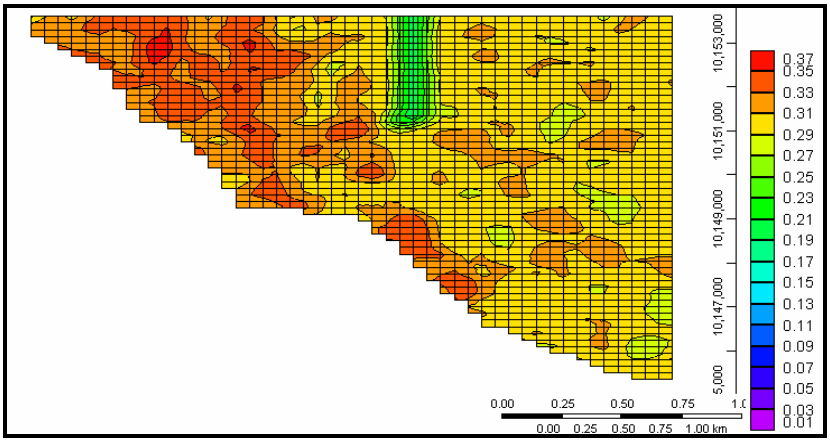

Fig. 48: Porosity distribution map (layer 1: observe the better development of western region).

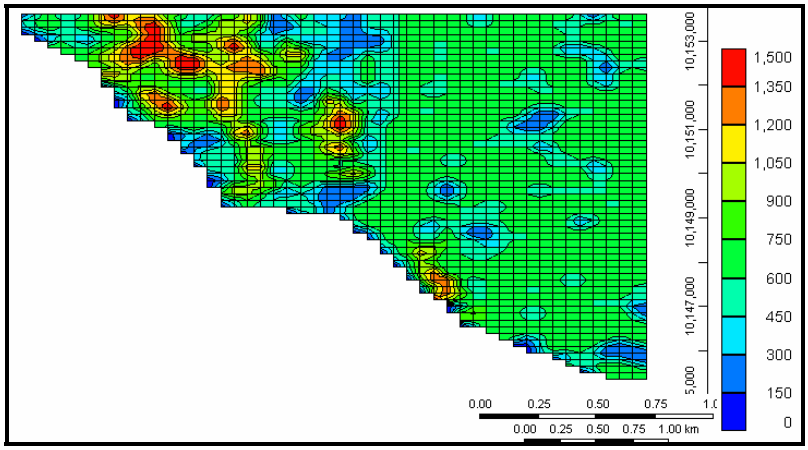

Fig. 49: Permeability distribution map (layer 1: again observe the better development of western region).

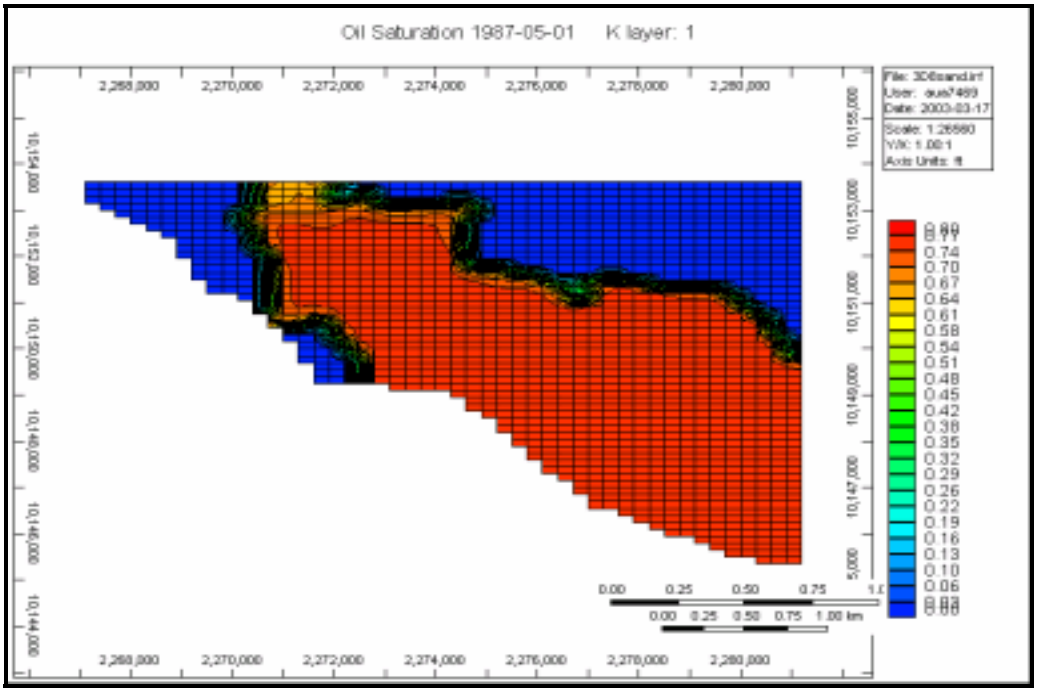

Fig. 50: Final static reservoir model (Initial oil saturation map).

Observe the gradation of the oil saturation close to the oil-water contact. This results from the capillary pressure influence: the simulator has been allowed to initialise the fluid distribution using the oil-water capillary pressure data.

CHAPTER IV

DYNAMIC RESERVOIR SIMULATION

Assumptions and Simplifications

Because of the complexity of the problem being solved, and to optimise time and resources, certain assumptions and simplifications were made in simulating the 8 reservoir. This permitted us to focus our resources on resolving the geological uncertainties that had hitherto posed the key uncertainties in delineating the reservoir and quantifying the reserves – a necessity in optimising the development of the reservoir.

The PVT data reported by the laboratory are assumed valid and used as are. The work was simplified significantly by this assumption, as it saved us sensitising, by varying the solution gas-oil ratio, R_s, on the size of the secondary gas cap and the effect of its expansion as a drive energy source. Another significant simplification from this assumption is that the effect of oil compressibility was not investigated, further reducing the number of uncertain parameters.

Each facies was assumed to have a single value of each of the properties - porosity, permeability in X, Y and Z directions, and net-to-gross ratio - in the fine grid system before upscaling. It was thought that no additional value would be added by doing a statistical distribution of the range of values of the properties for each facies. This is because upscaling the fine-grid model resulted in creation of unique values of each property in each grid block anyway.

Permeabilities in the X and Y direction are assumed equal. With the exception of the few areas where channels are present, vertical permeability, k_v, is generally assumed very low (less than 0.01 md).

The oil-water contact (OWC) encountered in well 3 is taken to be the OWC throughout the reservoir, regardless of its complex stratigraphy. This simplification was tested for validity by investigating the impact of the OWC on water breakthrough times and on the reservoir's average pressure profile. The single OWC at 10,310 ftss agreed the most with these match parameters.

History Matching

The dynamic simulator, CMG-IMEX, was used to simulate the production and pressure history of the reservoir. The history match process involved matching simulated average reservoir pressures and production volumes to historical static bottomhole pressures and cumulative reservoir production. This process validates the hydrocarbon pore volume present in the reservoir.

The concept of the history-match process was that we would first match global parameters like average reservoir pressure and overall reservoir production volumes, then match the water-cut and gas-oil ratio for individual wells. Fig. 51 shows a stack of the final match of key match variables at the reservoir level.

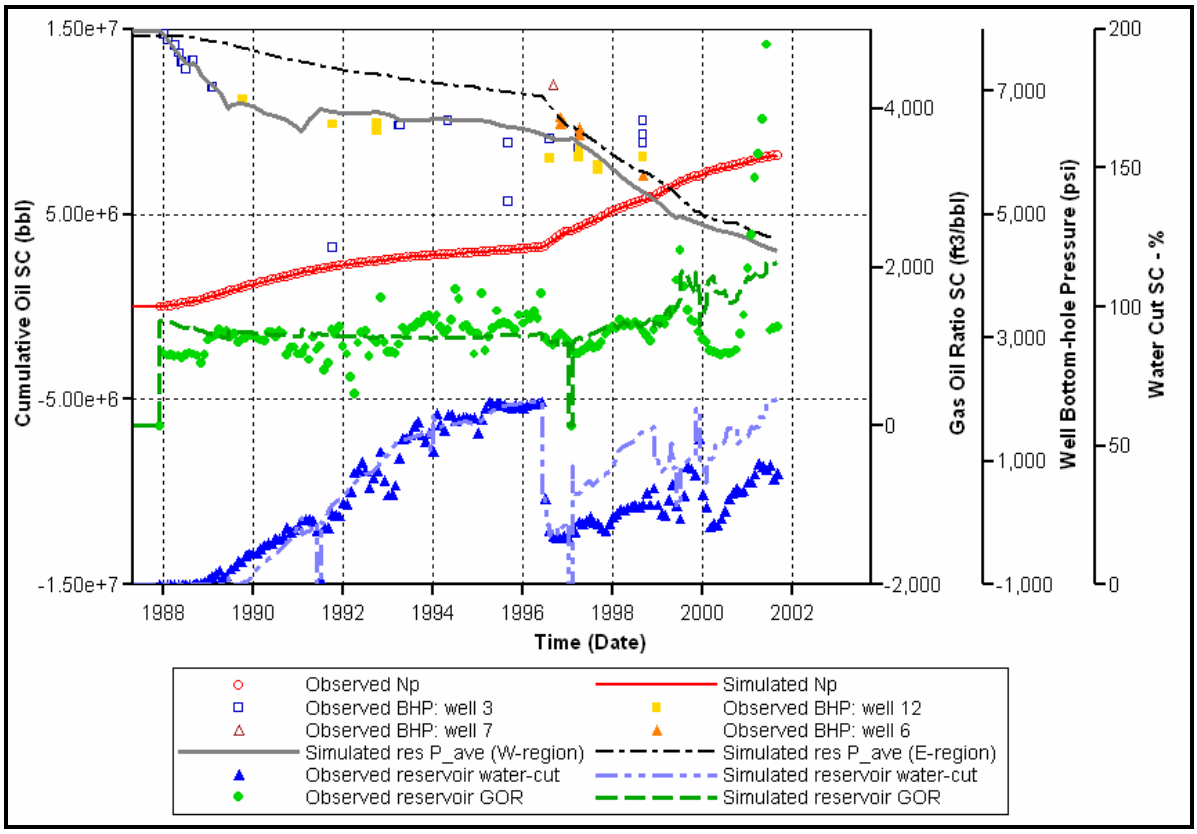

Fig. 51: Stack of the final history match of key variables – reservoir level.

Oil Production Match

The history-match has been constrained to the oil rate, hence the perfect match of the cumulative oil production. Matching the cumulative production at the reservoir level provided a qualitative determination of the range of permeability for the different facies. When matched for individual wells, the cumulative oil production match provided information on the spatial distribution of the facies within the drained volume of the wells. It also indicated the mobile oil volume available to each well.

Figs. 52, 53 and 54 show the cumulative oil production and oil rate match at reservoir level, and cumulative oil production match at well level, respectively.

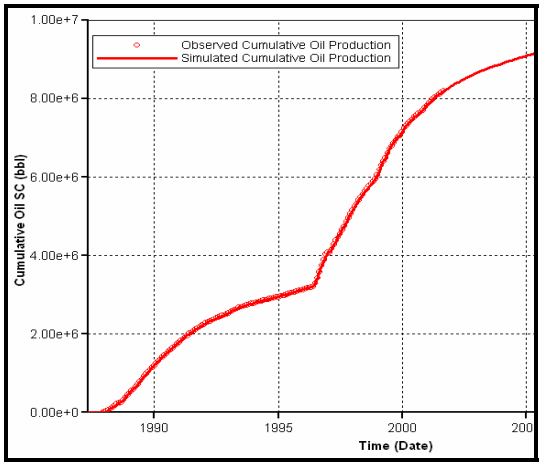

Fig. 52: History match of cumulative oil production at reservoir level.

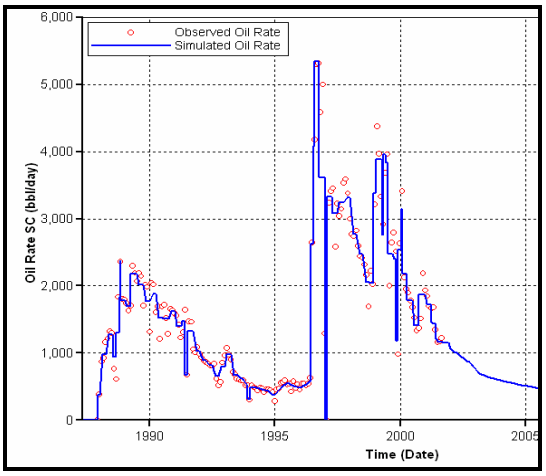

Fig. 53: Oil-rate match at reservoir level.

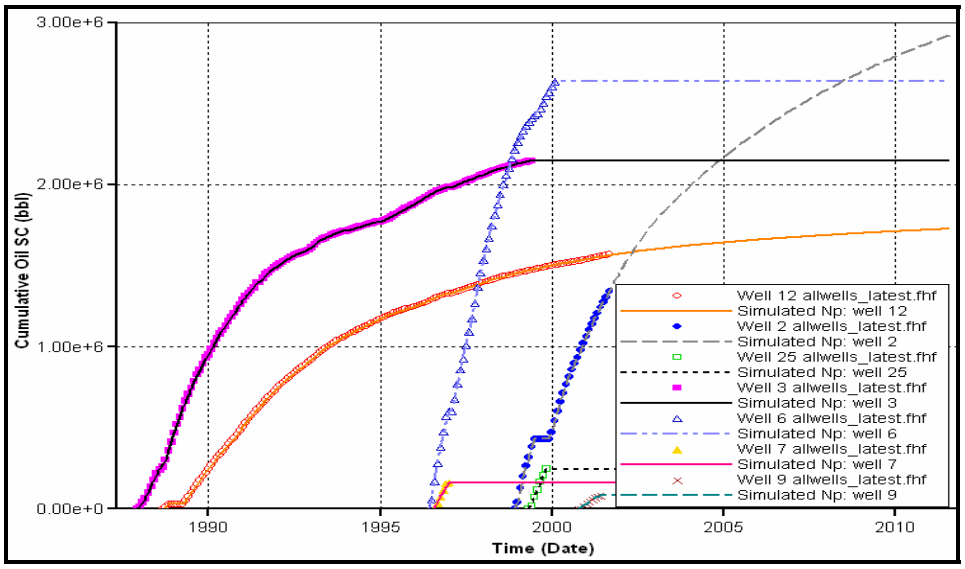

Fig. 54: History match of cumulative oil production at well level.

Pressure History Match

Matching the simulated average reservoir pressure to observed pressure history provided a means of evaluating the dominant drive mechanisms and sensitizing on the chronology of their individual or combined occurrence. Compaction drive was sensitised on by varying the rock compressibility relative to the degree of presence of other drive types. Water drive was modelled by attaching an aquifer. Varying the strength and transmissivity of the aquifer affected the average reservoir pressure and aquifer reaction times,

respectively. Ultimately, compaction drive delivered the best match in combination with other key parameters.

Observe the two match lines in Fig. 55 – the red continuous line and the maroon dashed line. Bottomhole pressure (BHP) data are available in only four wells, namely wells 3, 12, 7 and 6. The red and blue circles are the BHP data from wells 3 and 12, respectively, while the green and purple squares are the BHP data from wells 7 and 6, respectively. The red line is the simulated average reservoir pressure for the western region matching BHP data for wells 3 and 12, while the maroon dashed line is the simulated average reservoir pressure for the eastern region matching BHP data for wells 7 and 6. The two match lines were obtained by allowing a "low-transmissivity throat" of communication between the two regions. BHP pressure data from wells 3 and 12 in 1999 seem to suggest that the transmissivity of the throat may be even smaller than modelled. However, the investigation of the throat size was not further pursued because the said data showed considerable scatter.

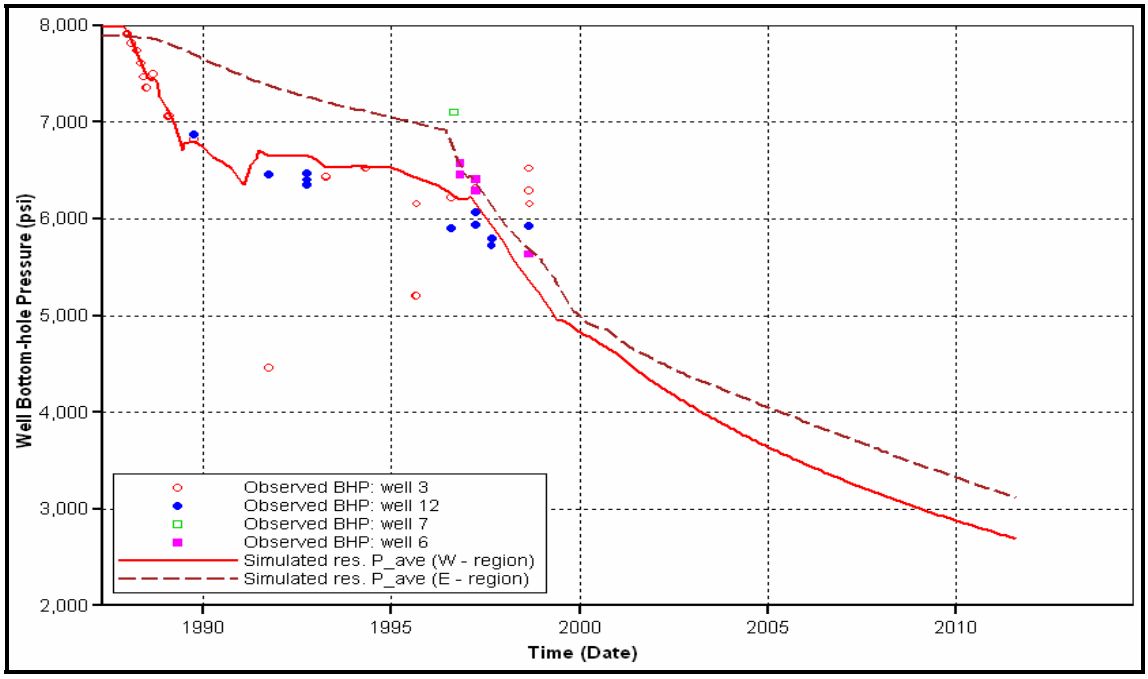

Fig. 55: Final history match of simulated average reservoir pressure to observed bottomhole pressure (the extension is the prediction of the base case).

The match between simulated average reservoir pressure and the bottomhole pressure history is excellent. The results of the investigation of the dominant drive types and capillary pressure profile indicated that there is a limit beyond which further attempts at improving the match of the historical production parameters is fruitless.

Water-Cut and Gas-Oil Ratio Matches

Water-cut and gas-oil ratio matches were most impacted by the end-point capillary pressure data and by its profile. Since the capillary pressure is a function of water saturation and this in turn is dependent on the facies, we conclude that the water-cut is influenced by facies distributions, especially their positions relative to the producing wells. The water breakthrough time and the water-cut profile are controlled by the capillary pressure end-point data and profile.

Another factor that affected the water-cut trend with time is the wells completion and recompletion history. An important factor to matching the water-cut and gas-oil ratio is the reservoir topography. The input of a geoscientist is required to modify this. We believe that the results of our calibration process should have prompted a re-evaluation of the seismic data and a re-interpretation of the inter-well distribution and extent of the facies. We surmise that this would have resulted in a much more improved geologic model. However, this desired rework was precluded by the sequential approach adopted in this study and the consequent lack of geoscientists at time the calibration process was completed.

Matching water-cuts and gas-oil ratios on a per-well basis provided the means to calibrate the geological parameters in the various realizations. It further enhanced the spatial distribution of the facies in the drainage volumes of the wells and provided information on the range of values of properties for the individual facies. Fig. 56 shows the water-cut match at the reservoir level. Figs. 57 through 59 show the water-cut matches on some of the producing wells.

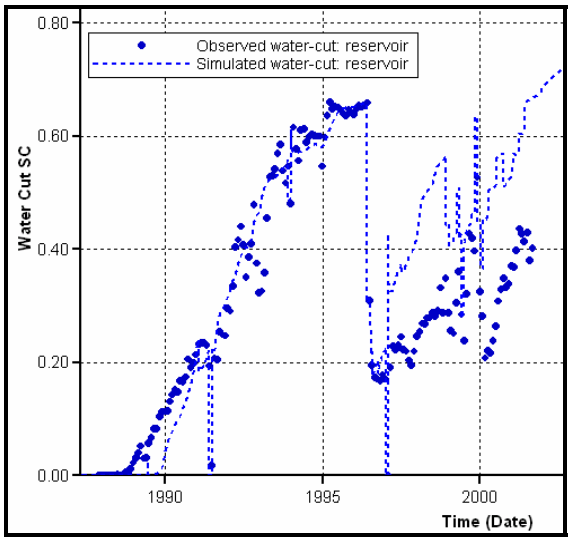

Fig. 56: Water-cut match: reservoir.

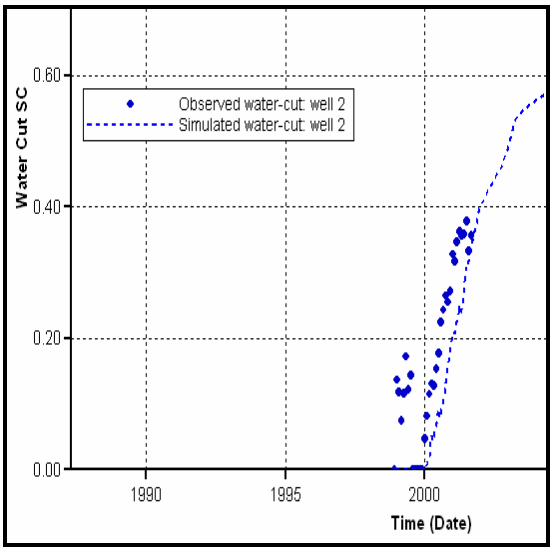

Fig. 57: Water-cut match: well 2.

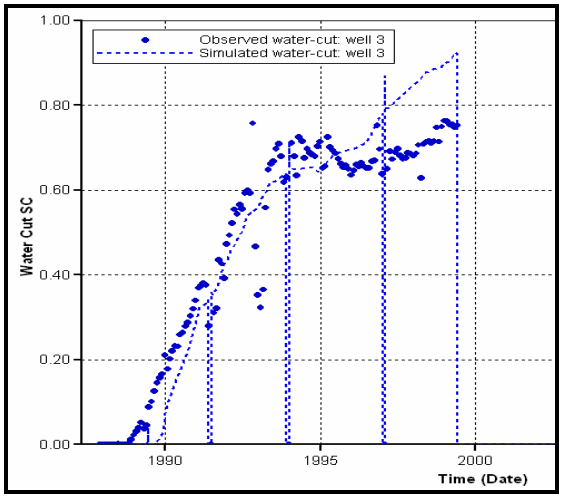

Fig. 58: Water-cut match: well 3.

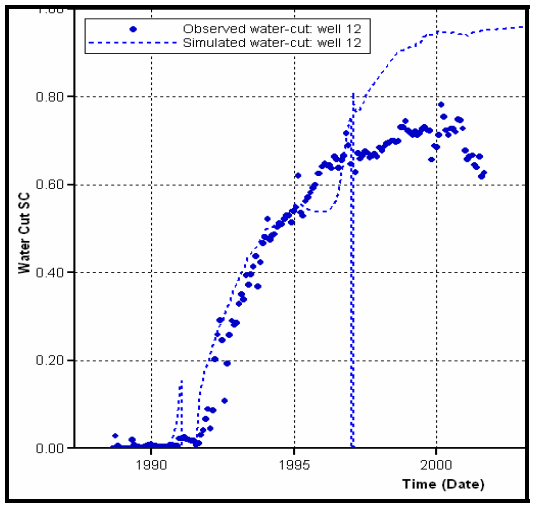

Fig. 59: Water-cut match: well 12.

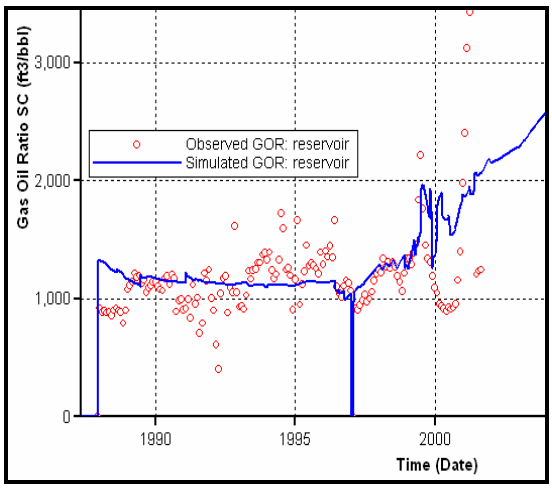

Fig. 60: History match of gas-oil ratio at reservoir level.

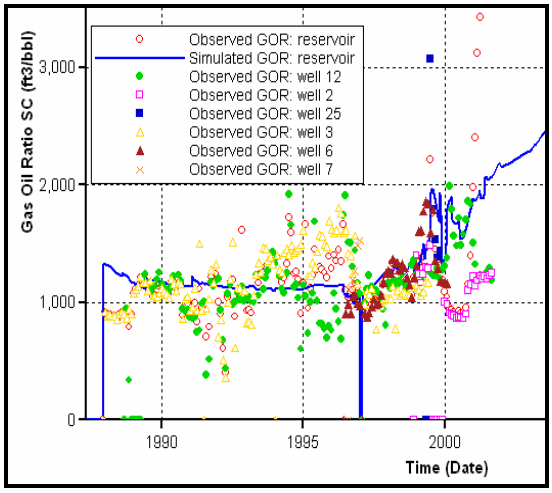

Fig. 61: History match of gas-oil ratio at reservoir level – with well GOR's overlain on it.

The observed GOR profile (Fig. 60) alludes to the reservoir possessing a more complex architecture than currently modelled. The rises and falls in the GOR profile in all the wells after the reservoir pressure fell below bubble point may suggest cyclic blow-down and oil-resaturation of the secondary gas cap (Fig. 61). This can occur due to entrapment of liberated solution gas in locations proximate to the producing wells. The jump from an initial GOR of ca 930 scf/stb to ca 1230 scf/stb supports this postulation. An alternate

reason could be that communication was established with another hydrocarbon accumulation with a higher GOR at the time of the jump. So far, we have discovered no evidence to support this postulation.

However, Fig. 62, which has the GOR from all the wells overlain on that of the overall reservoir GOR, shows that all the GOR's from the wells overlay themselves and that of the reservoir. This is rather unnatural and makes the observed GOR data suspect because the wells are located at different elevations relative to the reservoir crest and as such are expected to exhibit different GOR profiles.

Key History-Match Parameters

Several factors were key to matching the dynamic behavior of the 8 reservoir. The dominant drive energy (controlled by the rock compressibility, c_f, and the aquifer size and transmissivity), the capillary pressure and relative permeability profiles, the hydrocarbon pore volume (determined from the net-to-gross ratio and rock porosity), and the geological architecture had very significant influence on the reservoir performance.

The Dominant Drive Energy

The source of the significant drive energy observed in the reservoir pressure behavior was a key uncertainty in this work. We investigated three main drive types, namely depletion (or solution gas) drive, aquifer drive and compaction drive. We did not consider primary gas-cap expansion because the reservoir was originally undersaturated. The dominant drive mechanism determined not only the pressure behaviour, but also the displaceable oil, the water-cut behaviour, the gas-oil ratio behaviour, and the oil recovery factor. The sensitivity on the actual dominant drive type was done by running the geological model under three scenarios: one with high c_f and small aquifer (compaction drive case), another with a moderate-sized aquifer and small c_f, (aquifer drive case), and a third with small c_f and small connected water-leg (solution drive case).

Aquifer Support

The impact of water drive on the reservoir behavior is controlled by both the aquifer size and the aquifer transmissivity. The transmissivity determines the aquifer reaction time, and once the aquifer is felt, the magnitude of its influence is determined by its size. The presence of an aquifer has two effects on the water-cut, namely a) increasing the slope of the water-cut trend, and b) generally boosting the water-cut. An approximate match was obtained for the reservoir pressure behavior (Fig. 63). However, because matches on other parameters were persistently significantly off, we concluded that aquifer drive was not the active drive mechanism in the 8 reservoir.

Solution Gas Drive

Depletion (or solution gas) drive alone resulted in continuous pressure decline (Fig. 64). It did not yield a match on any of the other match parameters. Thus, we concluded that solution gas drive is not the primary drive type in this reservoir.

Compaction Drive

Special core analysis, SCAL, performed on cores from well 7 by Petroleum Testing Services, Inc., in mid-1987, indicated the rock compressibility from experiment to be circa $27x10^{-6}\ psi^{-1}$ for a normally pressured rock of the average 30% porosity obtained in the 8 reservoir. Accounting for the effect of overpressure, we have used the obtained value as our minimum and sensitized on higher values. A high rock compressibility of ca $49x10^{-6}\ psi^{-1}$ best reproduced the primary match parameters. As pore pressure decreases, some grain crushing occurs when grain-grain contact is established. This is accompanied by rock grain rearrangement with the grains forcefully displacing fluid out of the pore spaces. This compaction effect manifests as some pressure sustenance in the reservoir.

This drive type yielded the most acceptable match of all the history-match variables. We conclude that it is the dominant and active drive mechanism in the 8 reservoir.

Interpretation

The rapid pressure depletion observed early in the life of the reservoir resulted from two factors: single-phase depletion of the undersaturated oil, and the limited reservoir volume accessible in the period of the initial pressure measurements. When we consider that the reservoir consists of vertical and lateral alternations of sand and shale, a so-called compensational stacking sequence, we appreciate that only the sand bodies perforated in a well contribute to production. When we combine this knowledge with the fact that only well 3 was producing during the period of the observed early rapid pressure depletion, we realize that the BHP measured in the period returned only the pressure behavior of the fraction of the reservoir developed by well 3. The well is blind to the rest of the reservoir as a result of communication barriers caused by lithofacies discontinuities.

As more wells came on stream, more and more of this complex reservoir is accessed by wells for production, and assessed by BHP measurements in the wells. The apparent pressure sustenance that followed the early rapid decline resulted from the combination of this greater access to the reservoir and the effect of rock compaction.

Water production is observed in the 8 reservoir by virtue of the presence of a water leg. This water leg is of sufficient size to impact the reservoir pressure and production profile as a small and moderate-transmissivity aquifer. Increase in water cut is believed to result from pore-volume compaction of the water leg. Figs. 62, 63, 64 and 65 show the results of the three scenarios.

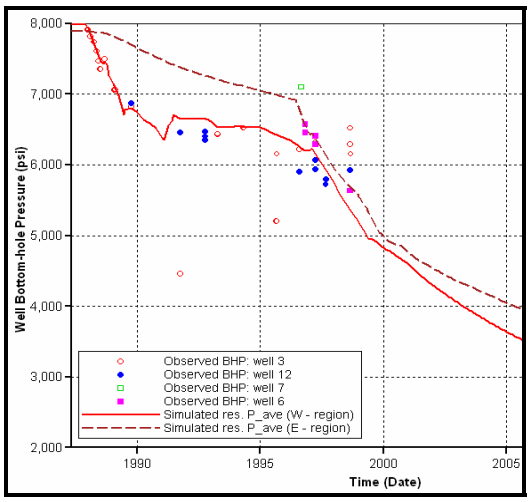

Fig. 62: Average reservoir pressure behavior with compaction (the two match lines are for the western region (red) and eastern region (dashed maroon), respectively.

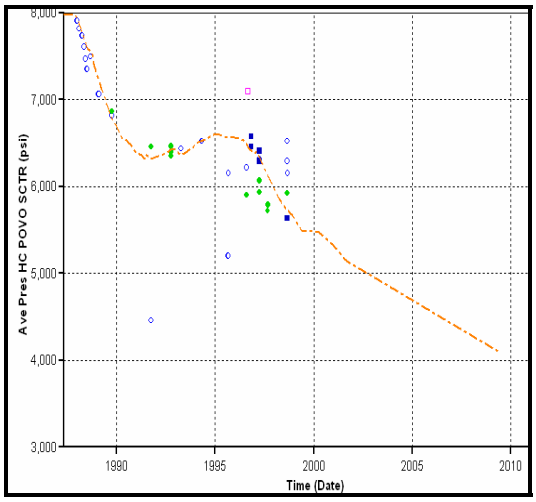

Fig. 63: Average reservoir pressure behavior with aquifer support (only western region match presented).

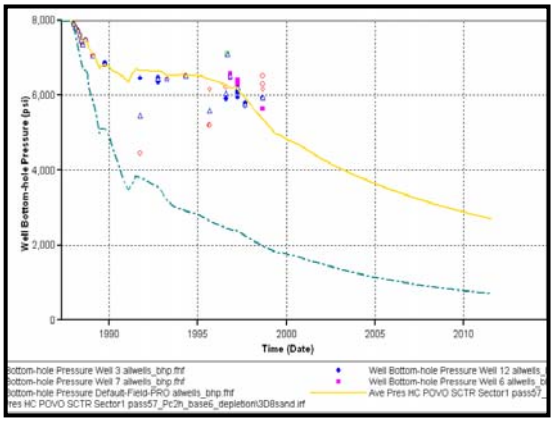

Fig. 64: Average reservoir pressure behavior under depletion drive mechanism (broken blue line) - (only western region match presented).

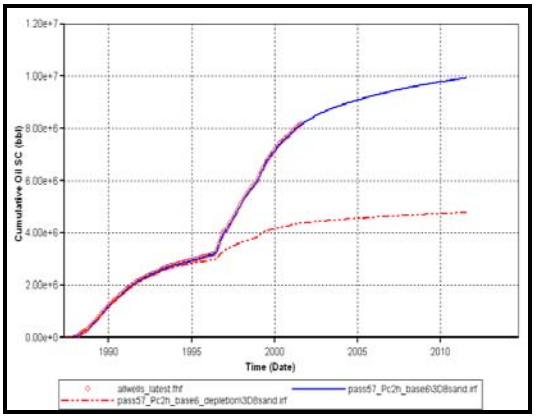

Fig. 65: Cumulative oil produced under depletion drive (broken red line).

Effect of Capillary Pressure and Relative Permeability Profiles

The capillary pressure profile with saturation and height above oil-water contact proved to be a key parameter that controlled the water breakthrough time and the water-cut profile. Consider that the capillary pressure profile can be represented by an expression with an index, say, n, ($n \geq 1$), where the index n increases with reservoir quality and pore throat size. Pore throat size is also indicated by the end-point

capillary pressure values, where the higher end-point values indicate poorer quality (smaller pore throat) reservoir. We discovered that varying the end-point values and changing the profile to indicate a poorer quality, smaller pore-throat-size reservoir increased the water-oil ratio and shortened the water breakthrough time in wells. In short, it enhanced the water imbibition process. The effects of the capillary pressure end-points and profile are illustrated in Figs. 66 and 67 for wells 2 and 3.

The markers are the observed water-cut profile for the wells. The blue continuous line is the match with capillary pressure profile and end-points indicative of high-quality, low-capillarity reservoir. The dashed grey line is the match with high capillary effects (low quality reservoir). All other parameters were unaltered. Observe that increasing the capillary pressure and decreasing the index *n* has the effect of boosting the water-cut and shortening the water breakthrough time. The same effect is observed in the other wells.

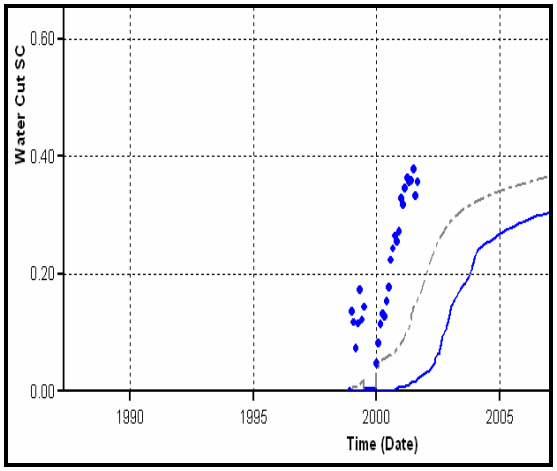

Fig. 66: Effect of capillary pressure on water-cut: well 2. The markers are the observed water-cut profile for the wells. The blue continuous line is the match with capillary pressure profile and end-points indicative of high-quality, low-capillarity reservoir. The dashed grey line is the match with high capillary effects (low quality reservoir).

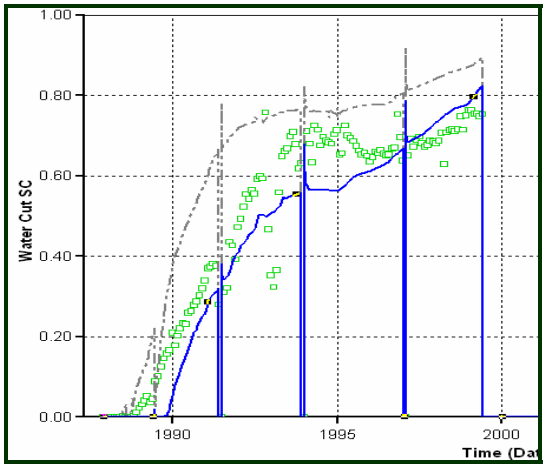

Fig. 67: Effect of capillary pressure on water-cut: well 3. The markers are the observed water-cut profile for the wells. The blue continuous line is the match with capillary pressure profile and end-points indicative of high-quality, low-capillarity reservoir. The dashed grey line is the match with high capillary effects (low quality reservoir).

Fig. 68 illustrates the effect of capillary pressure on the pressure profile. The simulated average reservoir pressure with capillary effects (all other parameters unaltered) shows lesser capacity to sustain itself with fluid withdrawal. This is essentially because of the lower total compressibility available due to the greater volume of water and lower volume of more compressible oil. The lower oil volume impacts the cumulative oil match as shown in Fig. 69 because there is lesser oil available for production.

The capillary pressure curves previously shown in Figs. 27 and 28 were used to obtain the final best-case history match.

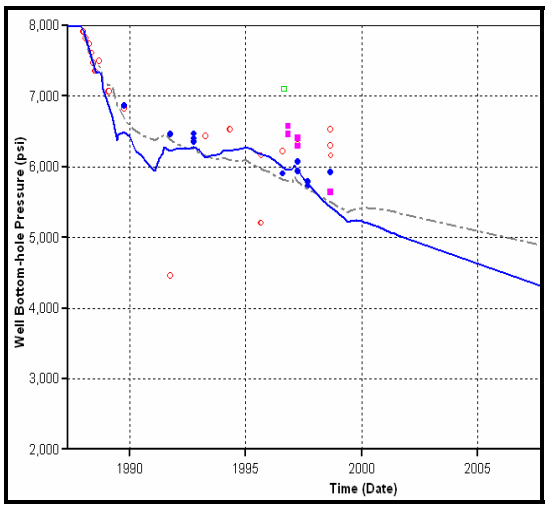

Fig. 68: Effect of capillary pressure on average reservoir pressure behavior. The markers are the observed pressure profile for the wells. The blue continuous line is the match with capillary pressure profile and end-points indicative of high-quality, low-capillarity reservoir. The dashed gray line is the match with high capillary effects (low quality reservoir).

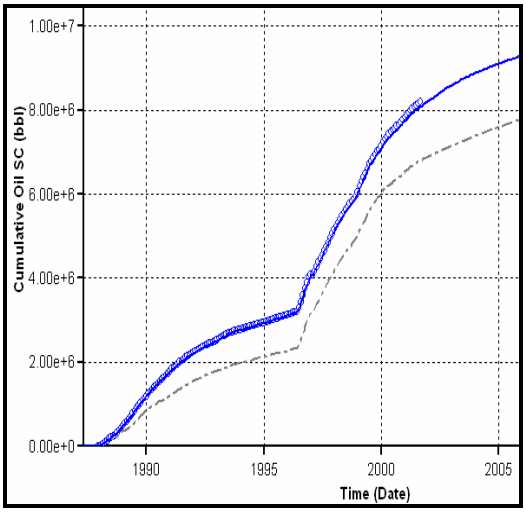

Fig. 69: Effect of capillary pressure on cumulative oil produced. The markers are the observed reservoir cumulative oil production. The blue continuous line is the match with capillary pressure profile and end-points indicative of high-quality, low-capillarity reservoir. The dashed gray line is the match with high capillary effects (low quality reservoir).

The Impact of the Completion History

The stratigraphy and architecture of the 8 reservoir is such that each sand layer constitutes a hydraulic unit, such that a layer must be perforated to be produced. Since the bottomhole pressure reported in a well depends on the compressibility of the total system the well is exposed to through its perforations, the implication of all the above is that the number of layers in which a well is completed impacts the pressure measured in the well and the total production from the well. Therefore, the completion and recompletion history of a well impacts not only its contribution to the reservoir performance, but also the performance of other wells producing any of the layers in which it is completed/recompleted.

It was necessary to recreate the completion and recompletion history of the wells before we could match the observed pressure behavior in the 8 reservoir.

CHAPTER V

FORECASTS FOR FURTHER DEVELOPMENT

Production forecasts were made to investigate future development and production strategies for the reservoir. Production predictions were made under four different operating scenarios:

1. A base case scenario in which the existing reservoir production strategy is maintained;

2. Further development of the reservoir with infill wells to drain the partially swept areas;

3. Further development of the reservoir with infill wells and with voidage replacement by water injection; and

4. Further development of the reservoir with infill wells and with voidage replacement by gas injection.

The benefits of each of the different development strategies were evaluated on the basis of the final oil recovery factor and incremental reserves.

The economic value of the combined cost of development and incremental revenue was not evaluated in this study. Fig. 70 compares the cumulative production under the four scenarios. Fig. 71 compares the reservoir average pressure behaviour under the four scenarios.

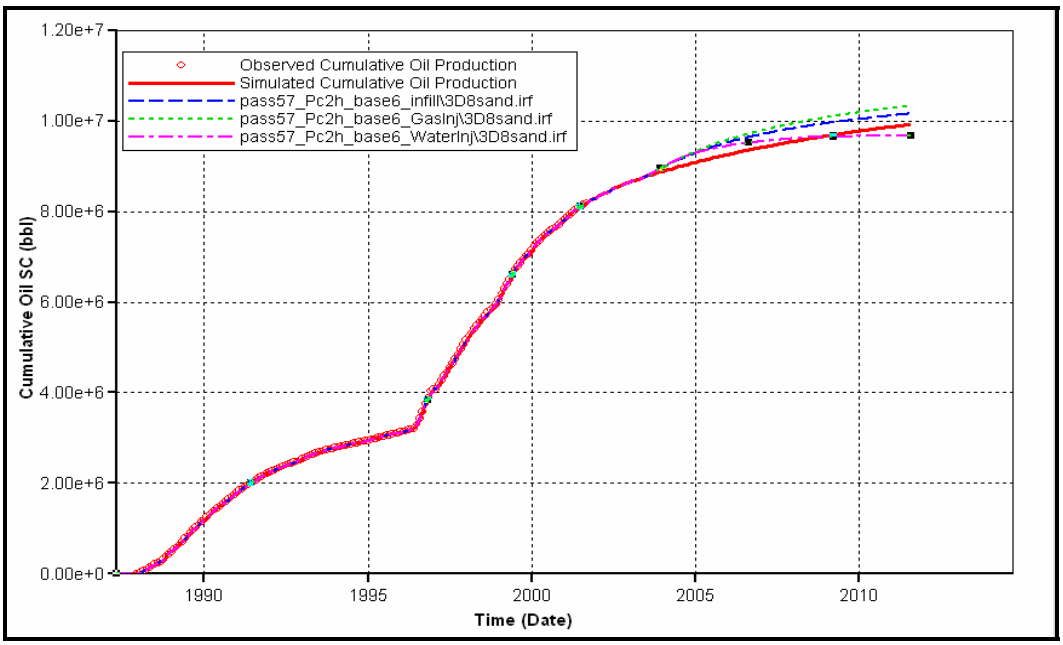

Fig. 70: Projected cumulative oil production history under the four redevelopment scenarios.

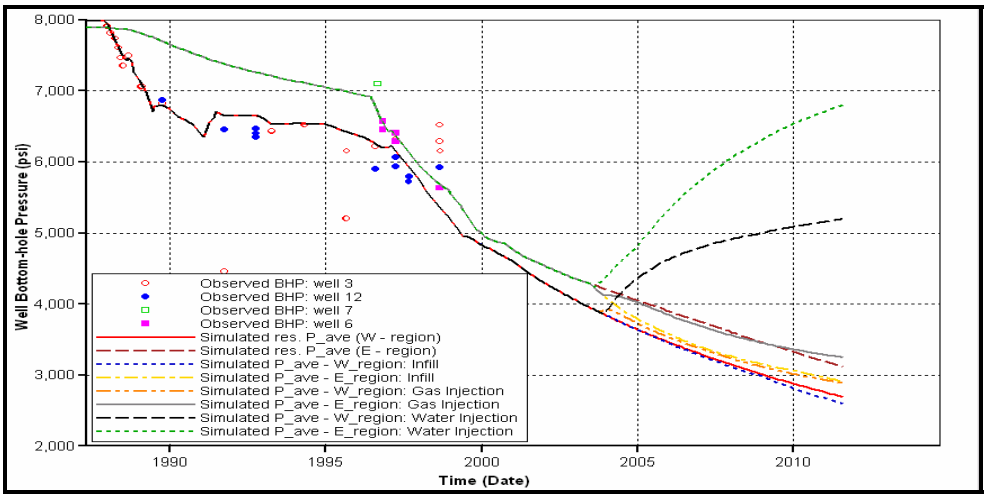

Fig. 71: Average reservoir pressure behavior under the four redevelopment scenarios.

The movie, Fig. 72 (animated by double-clicking on it), illustrates our justification for selecting infill and injection drilling locations for redevelopment options. It is the initial oil saturation map. The map illustrates the capillary-influenced gradation in the saturation close to the original oil-water contact. Double-clicking on the map animates it and portrays the advancement of water and the formation of a secondary gas cap. Further drilling activities are targeted at the areas with the high oil saturation at the end of history (Fig. 73).

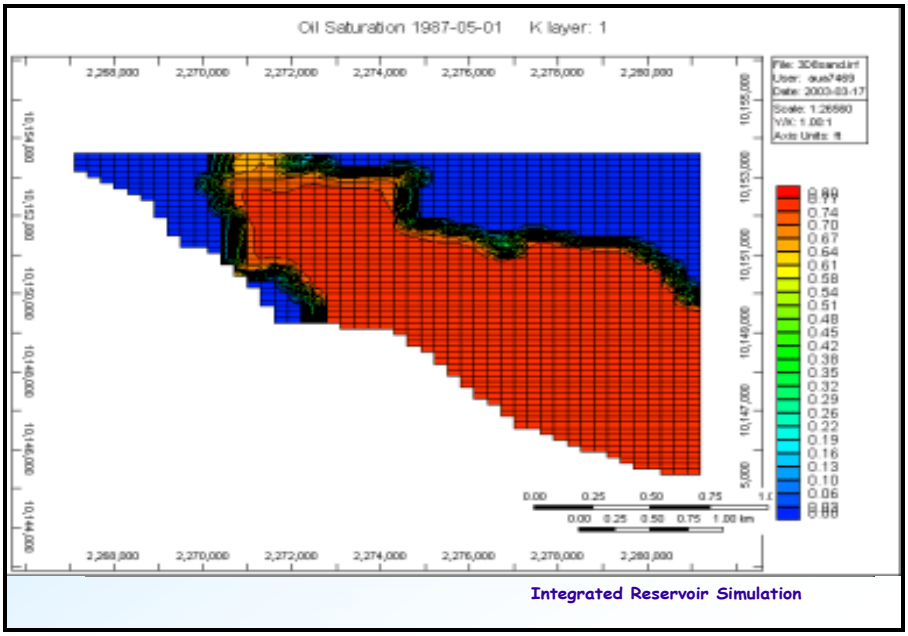

Fig. 72: Initial oil Saturation map. The map illustrates the capillary-influenced gradation in the saturation close to the oil-water contact. Double-clicking twice on the map animates it and portrays the advancement of water and the formation of a secondary gas cap. Further drilling activities are targeted at the areas with the high oil saturation at the end of history.

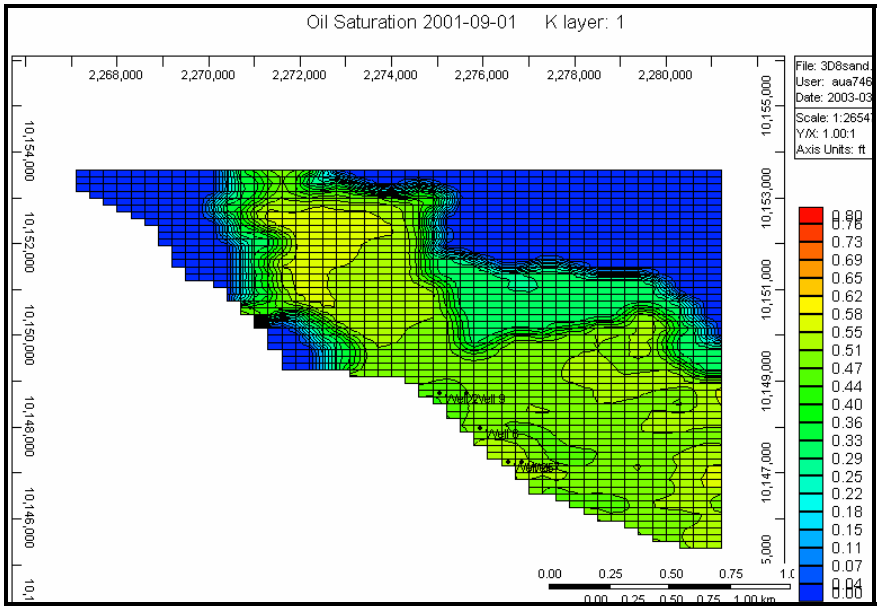

Fig. 73: Oil saturation at end of history (09/2001) – layer 1.

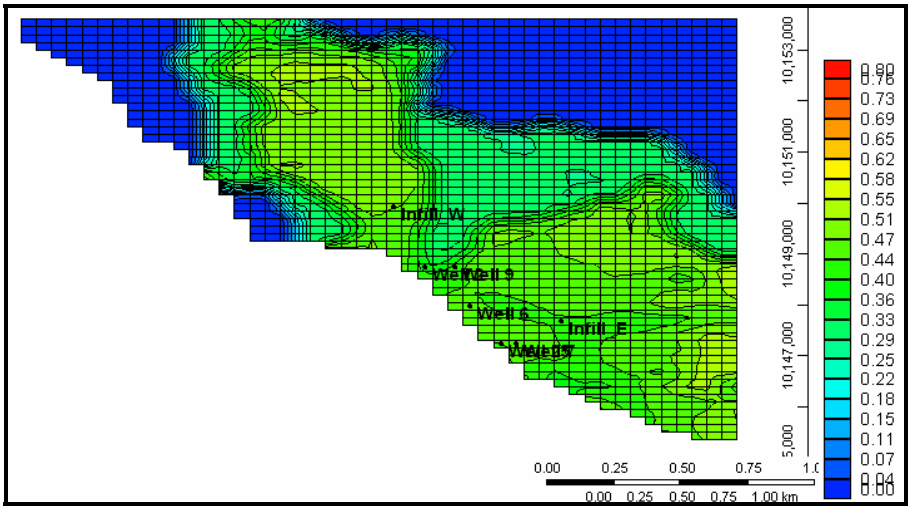

Fig. 74: Oil saturation map at end of history showing justification for choice of infill well locations.

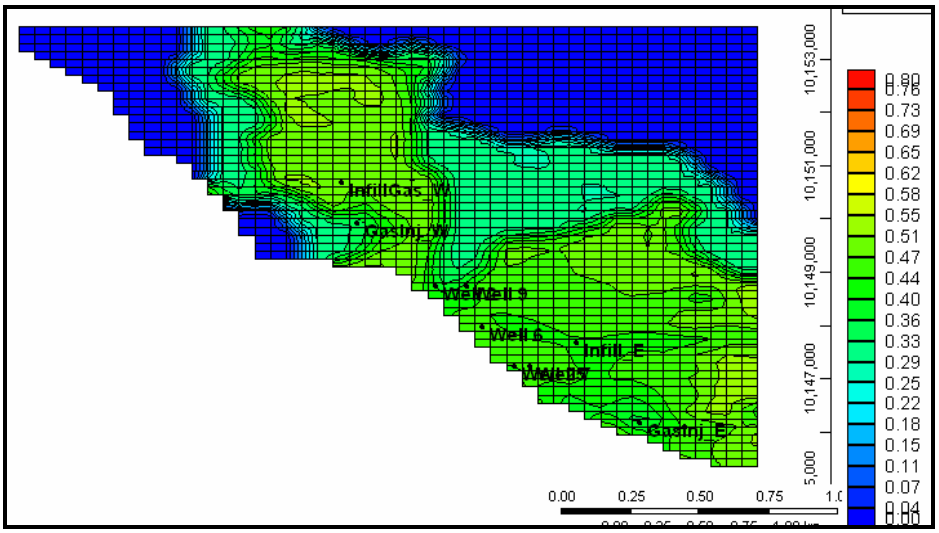

Fig. 75: Oil saturation map at end of history showing justification for choice of infill and gas injection well locations.

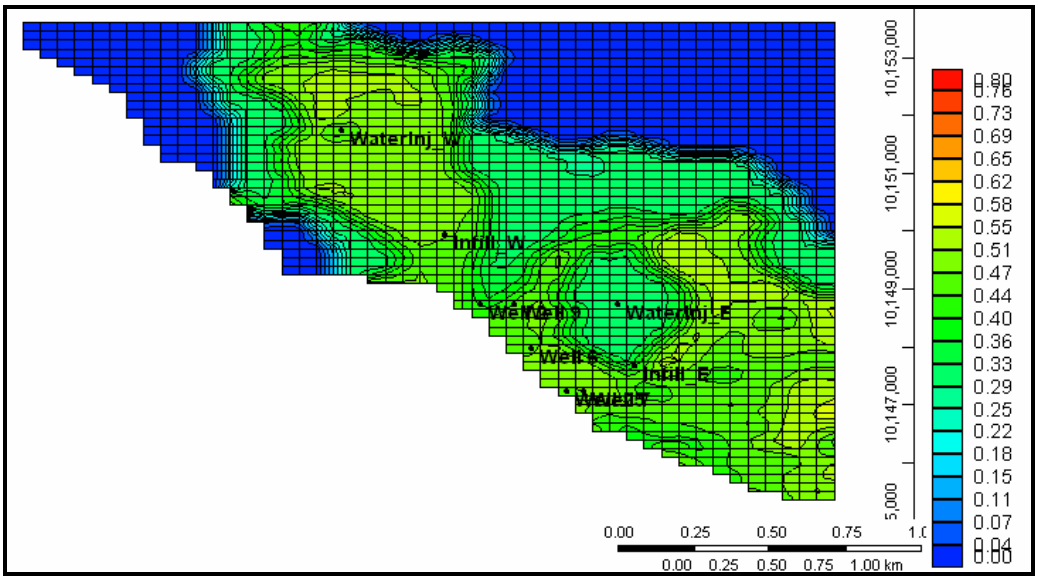

Fig. 76: Oil saturation map at end of history showing justification for choice of infill and water injection well locations.

Base Case

In this base case scenario, the existing reservoir production strategy is maintained with no human intervention to workover the wells for any reason.

As of 09/2001 some 8.19 mmstb, representing ca 41.3% of STOIIP, had been produced from the reservoir. A 10-year projection yields a cumulative recovery of ca 9.92 mmstb (a recovery factor, RF, of more than 50.11%), and reserves of 1.73 mmstb (Fig. 77). However, if, as it is hoped, the wells are worked over for recompletion purposes later in their production lives, the expected reserves should be substantially higher than presently determined.

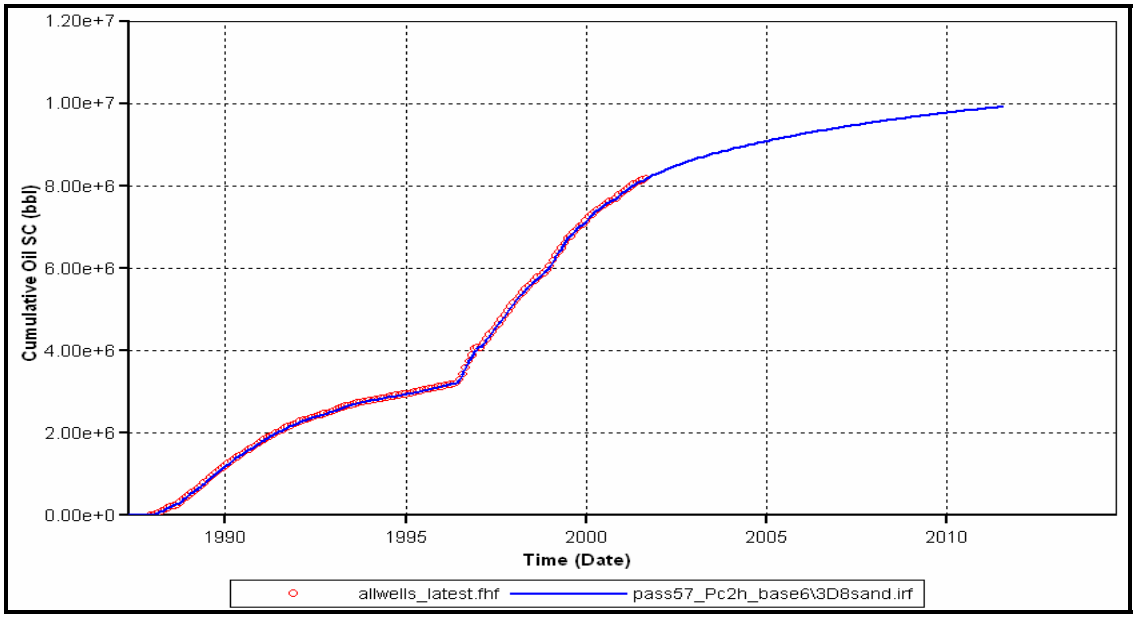

Fig. 77: 10-year projection of cumulative oil production under a base case scenario (no change in operations).

Infill Redevelopment

In this option two infill wells are drilled to drain poorly swept areas. Both wells are located in the eastern region of the reservoir. The infill well locations are chosen at the points of highest oil saturation at the time of the redevelopment. These locations were determined from observing the waterfront advancement and secondary gas cap formation in the two regions. Fig. 74 portrays the selected infill drilling locations. A 10-year projection, with the infill wells coming on stream 2 years into the projection period, yields a cumulative recovery of ca 10.16 mmstb (a RF of ca 51.3%) and reserves of 1.97 mmstb.

Enhanced Recovery with Gas Injection

In this scenario, further development of the reservoir is achieved with infill wells and with voidage replacement by gas injection. Two gas injection wells drilled in the local crests of the eastern and western

regions are employed for voidage replacement and to enhance the sweep of the remaining oil to the producing wells, inclusive of two additional infill producers (Fig. 75). The infill producing well locations are chosen at the points of highest oil saturation at the time of redevelopment. Fig. 75 portrays the selected infill and gas injection drilling locations. Gas injection constraints were set at maximum bottomhole pressure of 10,000 psi, and maximum injection rate of 2.0 MMscfpd per well. A 10-year projection, with the infill wells coming on stream 2 years into the projection period, yields a cumulative recovery of ca 10.33 mmstb (a RF of ca 52.18%) and reserves of 2.14 mmstb. Cumulative gas injection at the end of this 8-year injection period is 11.32 Bscf.

Enhanced Recovery with Water Injection

This strategy calls for further development of the reservoir with infill wells and with voidage replacement by water injection. Here, two water injectors are located to the flank of the producers (Fig. 76). Again, the infill well locations are chosen at the points of highest oil saturation at the time of redevelopment. Water injection constraints were set at maximum bottomhole pressure of 10,000 psi, and maximum injection rate of 10,000 bwpd per well. A 10-year projection, with the infill wells coming on stream 2 years into the projection period, yields a cumulative recovery of ca 9.66 mmstb (a RF of ca 48.8%) and reserves of 1.47 mmstb, indicating that waterflooding would be detrimental to the exploitation of oil from this reservoir. Cumulative water injection at the end of this 8 years injection period is 38.06 mmstb.

Best-Case Redevelopment Strategy

We acknowledge that determination of an optimal development plan hinges strongly on economic considerations. However, we did not conduct an economic analysis of the various development scenarios considered for the 8 reservoir in this study. This study was performed using data obtained through September 2001. Two additional wells have since been completed in the 8 reservoir; however, information from these two new wells has not been considered in this study.

Nevertheless, even without the benefit of an economic analysis, one can determine, by inspection, that a significant economic commitment is required to drill and complete four additional offshore wells and to install injection fluid handling and treatment equipment required for development-scenarios 3 and 4. Recently obtained cumulative production values through November 2002 showed an average 9-month contribution of ca 0.04 mmstb by the two additional new wells. Although this is consistent with the infill drilling case prediction reported herein, the disproportionately high additional investment for the infill drilling further justifies our choice of the base case as the best redevelopment case.

Therefore, based on technical considerations alone, there does not appear to be significant benefit to enhanced recovery operations. The base case appears to be the best case among the four redevelopment options considered for the 8 reservoir in this study.

CHAPTER VI

SUMMARY OF RESULTS

Calibration of the different geologic realizations, using history-matching, resulted in some convergence to a combined vertical and lateral stacking sequence model. Therefore, our final calibrated static model is one of a vertical and lateral stacking sequence. However, not having a geoscientist to implement this final model, the actual spatial distribution of the geological and petrophysical parameters representative of the 8 reservoir is still uncertain, albeit a lot less uncertain than before this work commenced. The degree of data misfit (though not significant) in the results of our efforts reflects this uncertainty.

Nevertheless, delineation of the hydrocarbon accumulation in the 8 reservoir was achieved by calibrating the oil-water contact through history matching. PVT data indicate that the reservoir was initially undersaturated, implying that it had no primary gas cap. The original fluids in place were determined to be 19.8 mmstb of oil and 26.2 Bscf of solution gas. Table 6 below summarizes the oil and gas volumes ultimately recoverable from the reservoir under the different scenarios we have considered for further development of the reservoir.

Table 6: Summary of production forecasts under four different development scenarios.

Scenario	Ultimate Recovery		Reserves		Infill well Requirement	Remarks
	Oil (mmstb)	Gas (bcf)	Oil (mmstb)	Gas (bcf)		
1. Base Case	9.92	16.01	1.74	5.99	Nil	
2. Infill without Secondary Recovery	10.16	16.80	1.97	6.78	2 wells	Minimum of 1 producer in each of the regions.
3. Infill with Water Injection	9.66	13.45	1.47	3.42	2 producers; 2 injectors	Minimum of 2 injectors: 1 in each of the regions.
4. Infill with Gas Injection	10.33	26.79 *	2.14	5.45 **	2 producers; 2 injectors	Minimum of 2 injectors: 1 in each of the regions.

* Total gas production including produced injected gas.

** Total gas produced minus G_p before injection minus G_{inj}.

The principal drive mechanism in the reservoir's early production life was depletion drive. However, as soon as the high-compressibility rock experienced sufficient pressure depletion to initiate pore pressure compaction, compaction drive dominated for the rest of the producing life of the reservoir.

The tabulated reservoir data sheet (Table 7) that follows summarizes the key reservoir data validated in this simulation and the final reservoir simulation results.

Table 7: Reservoir data sheet.

Field Name: Green Canyon 18	Field location: Offshore Louisiana in the GOM
Field Discovery Year: 1982	Total Number of Wells Drilled in Field: 30
Reservoir Name: 8 reservoir	Producing Formation: 8 reservoir
Field Area (Acres): 5888	Reservoir Datum Depth: 10,000 ftss
Reservoir Porosity: 12% - 37%	Depth Gas/Oil Contact: N/A
Reservoir Permeability: 10 md - 1500 md	Depth Oil/Water Contact: 10,310 ftss
Reservoir Net/Gross Ratio: 19% - 45%	Reservoir Temperature : 174 ^{o}F
Connate Water Saturation: 22% - 35%	Initial Reservoir Pressure: 7910 psi
Primary Drive Mechanism: Compaction	Reservoir Bubble Point Pressure: 7750 psi
Active No. of Production Wells (09/2001): 2 Active No. of Injection Wells (09/2001): none Horizontal/High Angle Wells: 1 / 7 (well 6 – >45^{o})	Reservoir R_{si} : 1323 scf/stb Reservoir B_{oi} : 1.533 rb/stb Oil Gravity: 32 ^{o}API
Estimated Ultimate Primary Recovery Factor (oil): 52 %	
Initial Reservoir Pressure Gradient: 0.791 psi/ft at 10,000 ftss (Reservoir was over 82% overpressured)	STOIIP: 19.8 mmstb GIIP: 26.2 Bscf
Cumulative Production, N_p : 8.19 mmstb oil Date : 09/2001	Ultimate Recovery (oil): 9.92 mmstb Ultimate Recovery (gas): 16.01 Bscf
Producing Formation Lithology, Diagenesis, Structural Style: Lithology: Fine-grained Turbidite sandstones alternating with shalestones. Stratigraphy: Vertical and lateral sand/shale stacking sequence (compensational stacking). Diagenesis: Sand is well worked by submarine currents. Structural Style: Submarine fan levee and overbank deposits cut in places by channels. Structural dip influenced by tectonics of nearby salt diapirs.	
Surface Facilities in Project Area: 900 ft Drilling/Production Platform in 760 ft of water. Capacity: 22,000 bopd; 25,000 bwpd and 45,000 to 60,000 Mscfgpd.	

CHAPTER VII

CONCLUSIONS AND RECOMMENDATIONS

1. The study has confirmed that the 8 reservoir in GC-18 consists of assemblages of vertical and lateral alternations of sand and shale, a so called compensational stacking sequence, comprising three facies, namely channel, levee and overbank deposits.

2. Combination of the unconsolidated matrix and abnormal pore pressure resulted in the reservoir experiencing severe compaction since its early production life. The principal drive mechanism in the reservoir is compaction drive.

3. The integrated multidisciplinary approach has yielded improved accuracy and process in characterizing inter-well reservoir heterogeneity. It facilitated the evaluation of key uncertain parameters, which in the case of the 8 reservoir are the rock compressibility, facies distribution, and capillary pressure.

4. There does not appear to be significant benefit to infill drilling or enhanced recovery operations. This conclusion is based on technical considerations only; no economic calculations were made.

5. The various resource volumes of the reservoir are tabulated below (Table 8) for the recommended option:

Table 8: Gas and oil resource volumes in the 8 reservoir as of 09/2001.

STOIIP		Ultimate Recovery		Reserves as of 09/2001		Remarks
Oil (mmstb)	Gas (bcf)	Oil (mmstb)	Gas (bcf)	Oil (mmstb)	Gas (bcf)	
19.8	26.2	9.92	16.01	1.74	5.99	Base case option.

6. The study has provided us with useful information about the production behavior of the unconsolidated, geopressured, thin-bedded 8 reservoir, deposited in a submarine fan environment, with respect to its drive mechanism and capillary pressure behavior. Only a high rock compressibility of ca $49x10^{-6}$ psi^{-1} effectively reproduced the primary match parameters. Though the reservoir exhibited a low net-to-gross ratio, its dynamic behavior exhibited low capillary effects, supporting the petrophysical and geological description of the individual sand beds being clean and of high quality.

NOMENCLATURE

SYMBOL		Description
B_{oi}	=	formation volume factor of oil at initial conditions (rb/stb)
c_f	=	rock compressibility factor (psi^{-1})
c_o	=	oil compressibility (psi^{-1})
k_{row}	=	drainage process - relative permeability to oil: water is the wetting phase (fraction)
k_{rw}	=	imbibition process - relative permeability to water: oil present (fraction)
N_p	=	cumulative oil produced
n	=	an index indicating reservoir quality in the capillary pressure profile
p_b	=	reservoir oil bubblepoint pressure (psia)
p_c	=	capillary pressure (psi)
p_i	=	initial reservoir pressure (psia)
q_o	=	oil rate
S_w	=	water saturation
S_{wc}	=	connate water saturation
T_{res}	=	reservoir temperature (^oF)

REFERENCES

1. Weimer, P., *et al.*: "Developing and Managing Turbidite Reservoirs: Case Histories and Experiences: Results of the 1998 EAGE/AAPG Research Conference," AAPG Bulletin, (2000), **84**, No. 4, 453-465.

2. Bouma, A.H., Normark, W.R., and Barnes, N.E.:, *Submarine fans and related turbidite systems*, Springer-Verlag, New-York, (1985), 351.

3. Weimer, P., *et al.*: "Atlas of Petroleum Fields and Discoveries, Northern Green Canyon, Ewing Bank, and Southern Ship Shoal and South Timberlier Areas (Offshore Louisiana) Northern Gulf of Mexico," AAPG Bulletin, (1998), **82**, No. 5B, 878-917.

4. "Development Plan and Geological Program, Green Canyon 18 Field," Mobil Exploration and Producing, United States, Inc., New Orleans, Louisiana, (June 1994).

5. "Mobil Reservoir Management Reference Manual: Green Canyon 18 Field," Mobil Exploration and Producing, United States, Inc., New Orleans, Louisiana, (May 1996).

6. Lalande, S.: "Characterization of a Thin-Bedded Reservoir in the Gulf of Mexico: An Integrated Approach," M.S. thesis, Geophysics, Texas A&M University, (2002).

7. Plantevin, M.: "Characterization of the 3-D Properties of the Fine-Grained Turbidite 8 Sand Reservoir, Green Canyon 18, Gulf of Mexico," M.S. thesis, Geology, Texas A&M University, (2002).

8. Karlo, J.F., and Shoup, R.C.: "Classification of Syndepositional Systems and Tectonic Provinces of the Northern Gulf of Mexico," Adaptation for Online Presentation from Poster Session at Houston Geological Society Dinner meeting, (February 7, 2000), www.searchanddiscovery.com/documents/karlo.index.htm, accessed December 2002.

9. McBride, B.C., Weimer, P., and Rowan M.G.: "The Effect of Allochtonous Salt on the Petroleum Systems of Northern Green Canyon and Ewing Bank (Offshore Louisiana), Northern Gulf of Mexico," AAPG Bulletin, (1998), **82**, No. 5B, 1083-1112.

10. Zhang, H.: "Salt Tectonics and Sequence Stratigraphy of Central Offshore Louisiana, Gulf of Mexico," PhD Dissertation, Oceanography, Texas A&M University, (1994).

11. Weimer, P. *et al.* : "Evaluating the Petroleum Systems of the Northern Deep Gulf of Mexico through Integrated Basin Anaysis: An Overview," AAPG Bulletin, (1998), **82**, No 5B, 865-877.

12. Varnai, P.: "Three Dimensional Seismic Stratigraphic Expression of Pliocene-Pleistocene Turbidite Systems, Northern Green Canyon, Northern Gulf of Mexico," AAPG Bulletin, (1998), **82**, No. 5B, 986-1012.

13. Reading, H.G. and Richards, M.: "Turbidite Systems in Deep-Water Basin Margins by Grain Size and Feeder System," AAPG Bulletin, (1994), **78**, No. 5, 792-822.

14. Weimer, P. *et al*,: "Sequence Stratigraphy of Pliocene and Pleistocene Turbidite Systems, Northern Green Canyon and Ewing Bank (offshore Louisiana), Northern Gulf of Mexico," AAPG Bulletin, (1998), **82**, 918-960.

15. Davies, D. K., P. S. Hara, and J. J. Mondragon, 1999, Geometry, Internal Heterogeneity and Permeability Distribution in Turbidite Reservoirs, Pliocene California: paper SPE 56819, presented at the 1999 SPE Annual Technical Conference and Exhibition, Houston, 3-6 October.

16. "Green Canyon Block 18 Field: Detailed Sequence Stratigraphy Study," Subsurface Consultants & Associates, Inc., Lafayette, Louisiana (29 Nov. 1994).

17. Core Laboratories, Inc., "Special Core Analysis Study," for Mobil Exploration and Producing United States, Inc. New Orleans, Louisiana (December 1989).

18. Petroleum Testing Services, Inc., "Special Core Analysis Study," for Mobil Exploration and Producing United States, Inc. New Orleans, Louisiana (1987).

19. Weatherly Laboratories, Inc., "Reservoir Fluid Analysis Report," for Mobil Exploration and Production United States, Inc. New Orleans, Louisiana (February 1988).

20. "CMG – IMEX," Vers. 2002.1 Revision 4, (1978-2002), Computer Modeling Group, Toronto, Canada.

21. "GOCAD," Vers. 2.0.5, Release 2.0.5, (July 2002), Tsurf Technologies, Nancy, France.

VITA

Anthony Udegbunam Aniekwena

Education

B.Eng. Mechanical Engineering U. of Nigeria, Nsukka. Sept. 1987

High School: Kings College (Lagos, Nigeria) June 1982

Work Experience

7/01 to 8/01 Niger Delta Petroleum Resources (NDPR), Lagos, NIGERIA.

Responsibilities: Senior Petroleum Engineer

5/91 to 2/99 Shell Petroleum Development Company (SPDC), Warri, Nigeria.

Responsibilities: Reservoir Engineer

11/89 to 4/91 Shell Petroleum Development Company (SPDC), Warri, Nigeria.

Responsibilities: Well-site Petroleum Engineer

Permanent Address:

c/o Patrick Aniekwena
6271 Valley Bay Drive
San Antonio, TX 78250-5785